AGU PUBLICATIONS

Geochemistry, Geophysics, Geosystems

RESEARCH ARTICLE
10.1002/2013GC005144

Relationship between the Cascadia fore-arc mantle wedge, nonvolcanic tremor, and the downdip limit of seismogenic rupture

Patricia A. McCrory[1], Roy D. Hyndman[2], and J. Luke Blair[1]

[1]U.S. Geological Survey, Menlo Park, California, USA, [2]Pacific Geoscience Centre, Geological Survey of Canada, Sidney, British Columbia, Canada

Key Points:
- Cascadia fore-arc mantle corner located within band of tremor epicenters
- Slab depth associated with mantle corner and tremor varies along subduction zone
- 70 km wide gap exists between geodetic locked zone and fore-arc mantle corner

Supporting Information:
- ReadMe
- Figures ES1, ES2, ES3, ES4, ES5

Correspondence to:
P. A. McCrory,
pmccrory@usgs.gov

Citation:
McCrory, P. A., R. D. Hyndman, and J. L. Blair (2014), Relationship between the Cascadia fore-arc mantle wedge, nonvolcanic tremor, and the downdip limit of seismogenic rupture, Geochem. Geophys. Geosyst., 15, 1071–1095, doi:10.1002/2013GC005144.

Received 11 NOV 2013
Accepted 22 FEB 2014
Accepted article online 19 MAR 2014
Published online 22 APR 2014

Abstract Great earthquakes anticipated on the Cascadia subduction fault can potentially rupture beyond the geodetically and thermally inferred locked zone to the depths of episodic tremor and slip (ETS) or to the even deeper fore-arc mantle corner (FMC). To evaluate these extreme rupture limits, we map the FMC from southern Vancouver Island to central Oregon by combining published seismic velocity structures with a model of the Juan de Fuca plate. These data indicate that the FMC is somewhat shallower beneath Vancouver Island (36–38 km) and Oregon (35–40 km) and deeper beneath Washington (41–43 km). The updip edge of tremor follows the same general pattern, overlying a slightly shallower Juan de Fuca plate beneath Vancouver Island and Oregon (~30 km) and a deeper plate beneath Washington (~35 km). Similar to the Nankai subduction zone, the best constrained FMC depths correlate with the center of the tremor band suggesting that ETS is controlled by conditions near the FMC rather than directly by temperature or pressure. Unlike Nankai, a gap as wide as 70 km exists between the downdip limit of the inferred locked zone and the FMC. This gap also encompasses a ~50 km wide gap between the inferred locked zones and the updip limit of tremor. The separation of these features offers a natural laboratory for determining the key controls on downdip rupture limits.

1. Introduction

No great earthquakes (M81) have been instrumentally recorded on the Cascadia subduction zone, thus assessment of its seismic hazard requires evaluation and synthesis of indirect evidence. Rupture models typically estimate the spatial extent of the locked portion of the subduction fault where elastic strain which has accumulated since the last great earthquake ~1700AD is expected to be released in future damaging earthquakes. The potential for great earthquakes to dynamically rupture downdip from the inferred locked zone to where episodic tremor and slip (ETS) behavior is observed complicates efforts to characterize the seismic hazard. Nonetheless, the downdip limit of great earthquake rupture is key to accurate ground motion assessments, in part because the further downdip the subduction fault ruptures, the closer it approaches major urban centers such as Vancouver, British Columbia, Seattle, Washington, and Portland, Oregon.

For Cascadia, current seismic hazard assessments rest on integration of three main geological and geophysical data sets: (1) the distribution of paleo-seismic coastal subsidence, (2) the width of the geodetically inferred locked zone, and (3) the seismic-aseismic temperature threshold for felsic rocks along the subduction fault. Paleo-seismologic, geodetic, and thermal models provide a generally consistent downdip limit for significant rupture (herein defined as 1–2 m; 10% of maximum expected 10–20 m slip during great earthquakes) where the subducting Juan de Fuca plate reaches a depth of approximately 20–25 km [e.g., Hyndman, 2004, 2013] (Figure 1). For subduction systems with instrumental earthquake records, such as Sumatra, Chile and Japan, however, we find that significant seismic energy can be released both downdip [e.g., Briggs et al., 2006; McCaffrey, 2009] and updip [e.g., Simons et al., 2011] from the geodetically inferred locked zone during great earthquakes.

With the discovery of ETS along the subduction fault at depths of 35–45 km [e.g., Rogers and Dragert, 2003; Obara et al., 2004], where geodetic and thermal models had predicted continuous aseismic slip, our definition of the transition zone between episodic earthquake rupture and continuous aseismic slip has broadened to include this region where discrete slow slip events (SSE) and tremor attributed to shear slip have been observed [e.g., Ide et al., 2007; Wech and Creager, 2008; Obara, 2009; La Rocca et al., 2009, 2010]. These phenomena prompt us to revisit our assessment of the downdip limit of earthquake rupture, in particular, whether it extends to the updip edge of ETS. In addition, laboratory experiments indicate that serpentine and talc minerals associated with hydrated fore-arc mantle favor aseismic slip [e.g., Moore et al., 1997; Peacock and Hyndman, 1999], suggesting that the fore-arc mantle corner (FMC), where the upper plate of the subduction interface shifts from fore-arc crust to fore-arc mantle, may mark the extreme limit to rupture. Either of these potential constraints imply that coseismic rupture continues deeper than the otherwise defined limit.

The closest analog, the Nankai subduction zone beneath southwestern Japan, provides little insight into the relative importance of geodetic, thermal, ETS or FMC constraints as both tremor and the FMC occurs in close proximity to its geodetically and thermally inferred locking depths (Table 1). Conversely in Cascadia, geodetic and thermal constraints are widely separated from the ETS and FMC constraints under consideration. Thus, Cascadia potentially offers a natural laboratory to evaluate their relative significance.

In the following section, we briefly describe the three main data sets used to define rupture limits in Cascadia and their limitations. We then describe the two additional data sets to be evaluated in this contribution. In later sections, we briefly describe the seismic velocity data used to locate the fore-arc mantle corner and their limitations, followed by discussion of the methodology we employ to map the tremor and FMC and their uncertainties.

2. Models for the Landward Limit of Rupture in Great Cascadia Earthquakes

Current estimates of the downdip extent of significant rupture are based on simplified models of earthquake behavior. Paleo-seismic data are used to document the chronology and magnitude of past great earthquakes. Geodetic data are used to constrain the fault area expected to rupture in future great earthquakes. Thermal and rheologic data are used to predict its seismic or aseismic mode of slip.

2.1. Constraints Based on Paleoseismology

Abrupt Holocene land-level changes associated with Cascadia subduction earthquakes allow researchers to document the along-strike extent of prior earthquakes as well as their frequency of occurrence [e.g., Atwater et al., 1995; Leonard et al., 2004, 2010; Hawkes et al., 2011]. Holocene liquefaction and related features preserved in coastal marshes, lakes, and stream banks document the spatial distribution of strong ground shaking [e.g., Obermeier, 1995; Kelsey et al., 2005] which in turn allow estimates of where maximum fault slip occurred. Despite the painstaking construction of these chronologies, the geologic record for subduction earthquakes is likely incomplete. Land-level observations are limited to coastal zones, (including the east-west trending Strait of Juan de Fuca), where significant subsidence is marked by an abrupt change from terrestrial to estuarine habitat (often with an intervening tsunami-driven sand layer). Coastal marshes and lakes that record land-level changes are not evenly distributed along the Cascadia subduction margin. Furthermore, Holocene land-level changes integrate coseismic and postseismic movement. If significant postseismic slip (i.e., after-slip and visco-elastic relaxation) occurs downdip from coseismic rupture, the cumulative signal would indicate that rupture extended further landward than in fact occurred.

2.2. Constraints Based on the Interseismic Locked Zone

Coseismic rupture is expected to occur where the fault is locked and accumulating elastic strain (often expressed as a slip deficit) during the interseismic period. Recent great earthquakes off Sumatra and Chile support this premise: preshock estimates of the interseismic locked zone generally correspond with the coseismic rupture areas [e.g., Delouis et al., 2010; Shearer and Bürgmann, 2010; Loveless and Meade, 2011] albeit with significant heterogeneity in slip amount [e.g., Moreno et al., 2011]. Similar elastic dislocation models are used to map the degree and spatial extent of interseismic locking on the Cascadia subduction fault, and to estimate the accumulated slip deficit [e.g., Hyndman and Wang, 1995; McCaffrey et al., 2013]. Velocities between individual SSE, however, are faster than the longterm, averaged velocities [Holtkamp and Brudzinski, 2010] resulting perhaps in a fluctuating locking pattern, and raising the question of which velocity field should be used to determine the downdip extent of locking when the role of ETS is being evaluated.

The lack of geodetic observations on the seafloor above the offshore portion of the Cascadia subduction fault reduces the resolution of dislocation models. For example, the largest slip during the 2011 Mw9.0

Table 1. Comparison of Subduction Zone Characteristics

Subduction Zone	Oceanic Plate Age at Trench (Ma)	Plate Convergence Rate (mm/yr)	Locked Zone Downdip Depth (km)	Fore-Arc Moho Depth (km)	Depth to 350/450 (°C)	Tremor Depth Range (km)	Tremor Temperature (°C)
Cascadia/VI (JdF/NAm)	< 10[a]	45[a,b]	9[c]	35[d,e]	13/27[d,f]	25–45[g]	575[h]
Cascadia/WA (JdF/NAm)	< 10[a]	40[a,b]	10[c]	38–40[d,e]	13/27[d,f]	35–45[d,e]	525[i]
Cascadia/OR (JdF/NAm)	< 10[a]	35[a,b]	10[c]	33–40[d,e]	13/27[d,f]	30–40[d,e]	450[j]
Nankai/Shikoku (PhS/Pac)	15–25[k]	49[l]	30–40[m]	25–30[k]	28/42[n]	30–35[o,p]	500[p]
Nankai/Tokai (PhS/Pac)	15–25[k]	42[l]		25–30[k]	28/42[n]	40–45[o,p]	350[p]
Japan (Pac/Eur)	123[q]	91[r]	60–70[s,t]	32–35[u]	63/78[r]		
Sumatra (Ind-Aus/Sun)[v]	60[l]	45[l,x]	40[w,y]	21–25[l]	40/60[w]		

[a]Wilson [1993].
[b]McCrory [2000].
[c]McCaffrey et al. [2013].
[d]This paper.
[e]McCrory et al. [2012].
[f]Flück et al. [1997].
[g]Peacock et al. [2011].
[h]Peacock [2009].
[i]Oleskevich et al. [1999].
[j]Peacock et al. [2002].
[k]Kodaira et al. [2002].
[l]Dessa et al. [2009].
[m]Wallace et al. [2012].
[n]Seno [2005].
[o]Obara [2002].
[p]Hirose et al. [2008].
[q]Nakanishi et al. [1989].
[r]Peacock [2003].
[s]Suwa et al. [2006].
[t]Yamamoto et al. [2011].
[u]Doğan et al. [2006].
[v]VI denotes Vancouver Island; JdF denotes Juan de Fuca oceanic plate; NAm denotes North American continental plate; PhS denotes Philippine Sea oceanic plate; Pac denotes Pacific oceanic plate; Eur denotes Eurasian continental plate; Ind-Aus denotes Indian-Australian oceanic plate; Sun denotes Sunda continental plate.
[w]Klingelhoefer et al. [2010].
[x]30 mm/yr orthogonal component of convergence.
[y]seismogenic zone estimate based on thermal model.

Tohoku earthquake—as determined by integrated onshore and offshore observations—occurred where land-based geodetic models had previously inferred little to no offshore locking [Simons et al., 2011]. Since Cascadia lacks instrumentally recorded subduction earthquakes to verify whether the interseismic locked zone and accumulated slip deficit correspond to the coseismic rupture area and slip amount, we consider subduction systems where GPS measurements of deformation immediately following major subduction earthquakes allow us to make these comparisons in Section 5.

2.3. Constraints Based on Thermal Models

The abundance of quartz and feldspar appears to be a primary control determining downdip extent of seismic slip in felsic (continental) crust [e.g., Scholz, 1990; Blanpied et al., 1991, 1995]. Laboratory experiments document felsic rocks shifting from brittle to ductile deformation modes with increasing temperature [e.g., Blanpied et al., 1991, 1995], implying that a fault zone containing felsic minerals will similarly shift from seismic to aseismic behavior with increasing temperature. Seismic slip is expected until ~350°C. As the temperature increases from 350°C to 450°C, seismic slip propagating downdip is inferred to diminish while aseismic slip begins to predominate [e.g., Hyndman et al., 1997]. Above ~450°C, the fault is expected to slip aseismically [e.g., Hyndman and Wang, 1993].

In subduction settings, these temperature constraints are only relevant updip from the fore-arc Mohorovičić discontinuity (Moho) where the upper plate is composed of felsic material and the lower plate is composed of oceanic basalt. Further downdip, where eclogitized oceanic crust is in contact with an upper plate composed of either gabbroic lower fore-arc crust or peridotite fore-arc mantle, little felsic material is present. Because Eocene oceanic terranes make up a large portion of the Cascadia fore arc, the thermal properties of abundant mafic minerals such as pyroxene become important. Recent laboratory experiments document pyroxene gouge as maintaining brittle, stick-slip behavior up to ~550°C [He et al., 2013], implying a wider,

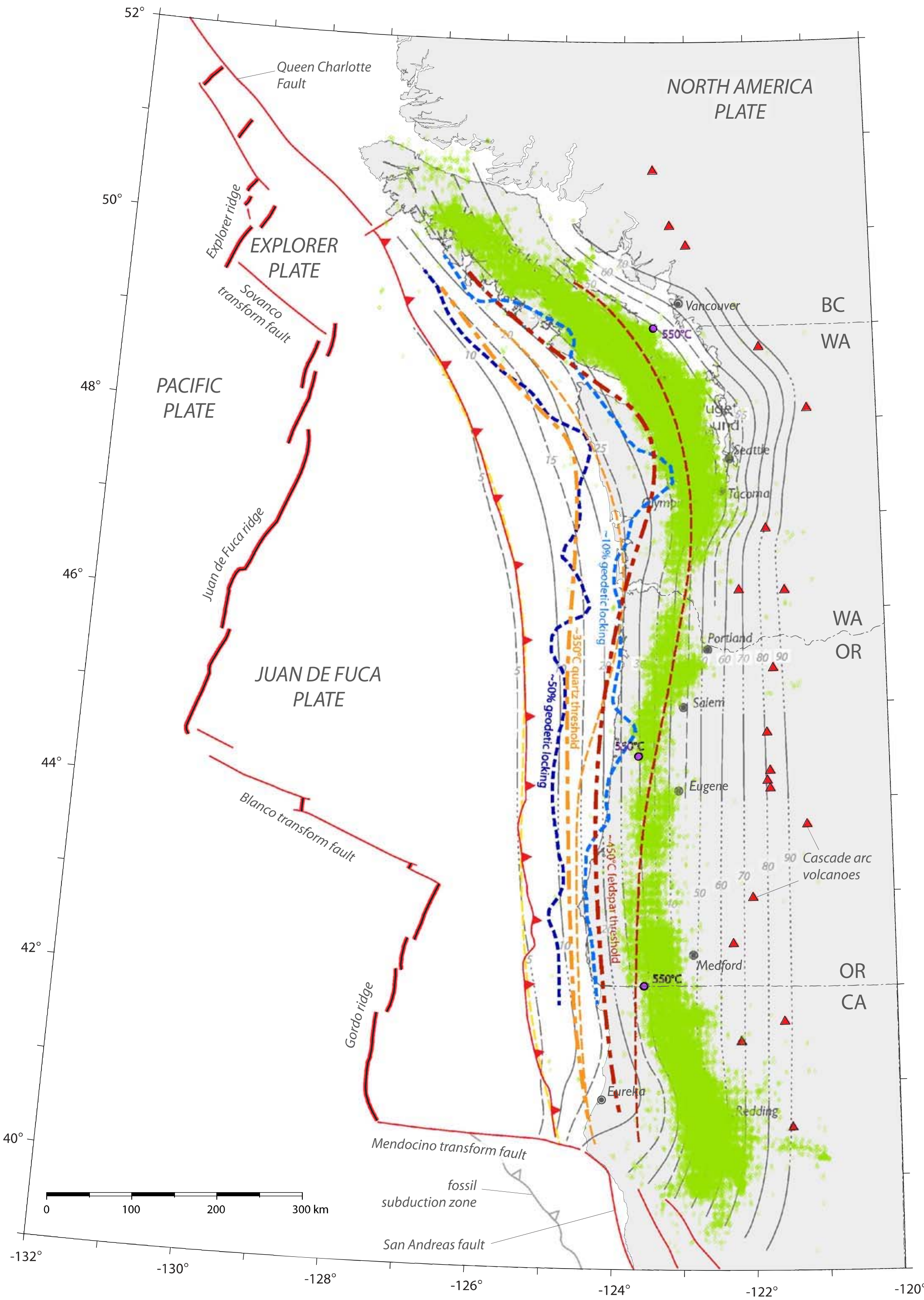

Figure 1. Map showing spatial distribution of tremor, denoted by green symbols (8 March 2010–8 March 2012; obtained from A. Wech, http://www.pnsn.org/tremor) and depth to the Juan de Fuca slab in km, denoted by gray contour lines from McCrory et al. [2012]. Quartz brittle-ductile threshold of 350°C denoted by dashed orange lines; and feldspar threshold of 450°C denoted by dashed red lines with thicker lines from Hyndman and Wang [1995] and thinner lines from Cozzens and Spinelli [2012]. Predicted slab temperatures of 550°C denoted by purple dots from Bostock et al. [2002], Peacock et al. [2002], and Peacock [2009]. Geodetically inferred 10% and 50% locking contours, denoted by dashed blue lines, modified from McCaffrey et al. [2013]. Gap discussed in text is located between 450°C contour of Hyndman and Wang [1995] or 10% locking depth and the updip edge of tremor.

thermally defined locked zone than published models predict. A 550°C thermal threshold for Cascadia would shift the thermally defined zone closer to the updip limit of tremor (Figure 1). He et al. [2013] proposed that tremor associated with mafic lower crustal rocks reflects unstable frictional behavior of gabbroic rocks which contain only trace amounts of quartz.

Thermal models provide an important, widely applied constraint on the downdip extent of seismogenic rupture, however, considerable uncertainty remains as to where these brittle-to-ductile mineral transitions occur along the Cascadia subduction zone. For example, thermal models that include the effect of hydrothermal cooling on the incoming Juan de Fuca plate shift the relevant isotherms as much as 10–15 km deeper Cozzens and Spinelli [2012] when compared to models that do not consider this parameter. Thermal models that include the effects of sedimentary prism thickening and fluid expulsion [Hyndman, 2013] currently provide a better fit to available heat flow data, thus, we use the Hyndman and Wang [1995] isotherms in our discussion below with the caveat that many key elements remain unresolved.

2.4. Constraints Based on Episodic Tremor and Slip

The updip or seaward edge of SSE has been proposed as a maximum bound for Cascadia earthquake rupture [e.g., Petersen et al., 2008; Chapman and Melbourne, 2009] based on the premise that strain within the ETS zone is primarily released aseismically by a combination of slow slip and other as yet undetected aseismic slip processes. Tremor serves as a reasonable proxy for SSE which are more difficult to detect and map. Tremor also indicates the presence of materials that can sustain brittle failure deep in the transition zone. Thus we focus on tremor in the discussion below.

ETS within Cascadia is commonly attributed to the presence of confined geo-fluids derived from relatively shallow dehydration of the Juan de Fuca slab [e.g., Abers et al., 2009; Boyarko and Brudzinski, 2010]. We assume that nonvolcanic tremor (NVT, sometimes termed tectonic tremor) and SSE are directly related since the two are closely correlated temporally and spatially [Bartlow et al., 2011], albeit NVT may not extend as far updip as SSE [Schmidt and Gao, 2010].

Temporally and spatially correlated NVT and SSE—downdip from the locked zone—have only been detected in the Nankai and Cascadia subduction systems to date [e.g., Schwartz and Rokosky, 2007]. Both subduction systems are characterized by relatively slow convergence of young, warm slabs (Philippine Sea plate is 15–25 Ma at the trench, Nankai convergence rate 20–40 mm/yr; Juan de Fuca plate is $<$ 9 Ma at the trench, Cascadia convergence rate 25–45 mm/yr; Table 1). SSE have been detected downdip from the locked zone in other warm subduction systems characterized by relatively slow subduction [Schwartz and Rokosky, 2007], including the Middle America subduction zone beneath southern Mexico (Cocos plate is 10 Ma at the trench; convergence rate 50 mm/yr) and the Central American subduction zone beneath Costa Rica (Nazca plate is 16 Ma at the trench; convergence rate 70 mm/yr) [McCaffrey, 1997; Verma, 2002; Kostoglodov et al., 2010; Boyarko and Brudzinski, 2010]. NVT has been detected in some of these subduction systems, but has not been directly correlated with SSE either spatially or temporally [e.g., Kostoglodov et al., 2010].

SSE have also been detected in a few cool subduction systems such as the Hikurangi subduction zone beneath northern New Zealand (Pacific plate is 100 Ma at the trench; convergence rate 40 mm/yr) and the Aleutian subduction zone beneath southeast Alaska (Pacific plate is 55 Ma at the trench; convergence rate 70 mm/yr) [e.g., McCaffrey, 1997; Schwartz and Rokosky, 2007]. Although NVT has not been detected in these subduction systems, instrumentation of most subduction zones is currently insufficient to presume that NVT is restricted to warm subduction systems. The exception is the cool Japan subduction system beneath northeastern Japan (Pacific plate is 123 Ma at the trench; convergence rate 91 mm/yr) [e.g., Nakanishi et al., 1989; Peacock, 2003] where—despite excellent instrumentation—neither SSE nor NVT have been detected.

2.5. Constraints Based on the Fore-Arc Mantle Corner

The FMC may mark the downdip limit of coseismic rupture in subduction systems where hydration of the fore-arc mantle wedge promotes aseismic slip along the subduction fault [e.g., Peacock and Hyndman, 1999; Bostock et al., 2002]. Alteration products associated with mantle hydration such as serpentinite, brucite, and talc exhibit stable sliding behavior at plate velocities [e.g., Moore et al., 1997; Moore and Lockner, 2007, 2008], thus tend to impede seismogenic rupture into regions where hydrated fore-arc mantle composes the upper plate of the subduction interface [Bostock et al., 2002].

The hydration state of a fore-arc mantle wedge can be estimated from heat flow data since serpentinization is associated with cooler than expected temperatures [e.g., Peacock et al., 2011]. Hydration state can also be inferred from seismic velocity studies that indicate lower than expected compressional (Vp) and shear wave velocities (Vs) for unaltered lithospheric mantle [e.g., Christensen, 1966, 1996, 2004; Peacock et al., 2011; Yamamoto et al., 2011; Ramachandran and Hyndman, 2012] as well as higher than expected seismic attenuation (1/Q), Poisson's ratios and Vp/Vs values. Since hydrated fore-arc mantle and noneclogitized oceanic crust have similar velocities, calculation of Poisson's ratio is key to distinguishing them because oceanic crust will have a much lower Poisson's ratio. Moreover, this ratio values allow calculation of the relative volume of serpentine within fore-arc mantle.

3. Data Used to Locate the Fore-Arc Mantle Corner

We constrain the location of the FMC using published seismic structure data derived from: (1) wide-angle active source experiments (mostly 2-D Vp profiles), (2) seismic tomography inversions (2-D slices through 3-D Vp models) of active source data, and (3) receiver function transects (providing 2-D dVs/Vs profiles) from temporary passive arrays recording distant earthquakes. Few seismic structure profiles have long enough baselines to reach the FMC. In particular, we have no profiles that reach the Moho in the southern portion of the Cascadia subduction zone (Figure 2). Where available, we synthesize deep seismic velocity data to map the depth of the fore-arc Moho with respect to the McCrory et al. [2012] Juan de Fuca plate model.

3.1. Determination of Moho Depth From Wide-Angle, Active Source Experiments

The Cascadia fore arc Moho is typically delineated as a sharp increase in Vp, from ∼6.8 km/s in the lower crust to ∼7.8 km/s in the upper mantle. This relatively low velocity (cold unaltered mantle typically has a velocity of ∼8.2 km/s) [e.g., Christensen and Mooney, 1995] impedes identification of the Moho in Oregon and Washington where fore-arc basement consists of the Siletz and Crescent oceanic terranes with relatively fast lower crustal velocities.

We constrain the FMC beneath southern Vancouver Island using two wide-angle refraction/reflection studies. The first set of Moho depths is derived from Nedimović et al. [2003] who merged several reflection lines from onshore and offshore surveys conducted in 1984 (Lithoprobe), 1985 (Frontier Geoscience), 1989 (Ocean Drilling Project, ODP), and 1998 (Seismic Hazards in Puget Sound, SHIPS) to construct a 160 km long NE-trending transect and a 220 km long SE-trending transect (Figure 2). Nedimović et al. extracted compressional wave velocities for these profiles from a 3-D tomographic model [Ramachandran, 2001], constructed by simultaneously inverting Vp first arrivals from the 1998 SHIPS experiment and regional earthquakes. They tentatively identified a horizontal Moho ∼34 km deep on the northern line and ∼44 km deep on the southern line (Table 2), based on wide-angle reflections from the Moho near the FMC. The landward extent of a band of prominent reflectors, termed the "E reflection band" or "E seismic layer," ends abruptly where the fore-arc mantle wedge intersects the subduction fault.

The second set of Moho depths is derived from Graindorge et al. [2003] who combined wide-angle and vertical incidence seismic velocity data from the 1998 SHIPS experiment with gravity modeling and regional seismicity to construct two NE-trending profiles, a 160 km long structural model across southern Vancouver Island and a 120 km long model across the Strait of Juan de Fuca and southernmost Vancouver Island (Figure 2). By including an ultramafic layer interpreted as Crescent mantle, Graindorge et al. depict a thicker Crescent terrane beneath Vancouver Island than many workers. We prefer their interpretation, and in turn, a somewhat deeper Moho because of the similarity in seismic signature between the Oregon reflective zone (discussed below) and the E seismic layer. Their Moho depths of ∼35 km for the northern transect and ∼44 km for the southern one (Table 2) are consistent with the Nedimović et al. [2003] depths. The deeper Moho on the southern transects of both Nedimović et al. and Graindorge et al., however, is not well resolved.

We constrain the FMC beneath Washington using two wide-angle refraction/reflection studies. The first set of Moho depths is derived from Miller et al. [1997] who constructed a north-south, 280 km long profile from a 1991 (Western Cascades) wide-angle refraction/reflection experiment through the Puget Sound region (Figure 2). Although the transect was situated east of the FMC, Miller et al. [1997] imaged the Moho just east of the FMC at ∼42 km depth at the northern end of their profile. Their velocity model (derived from

10.1002/2013GC005144

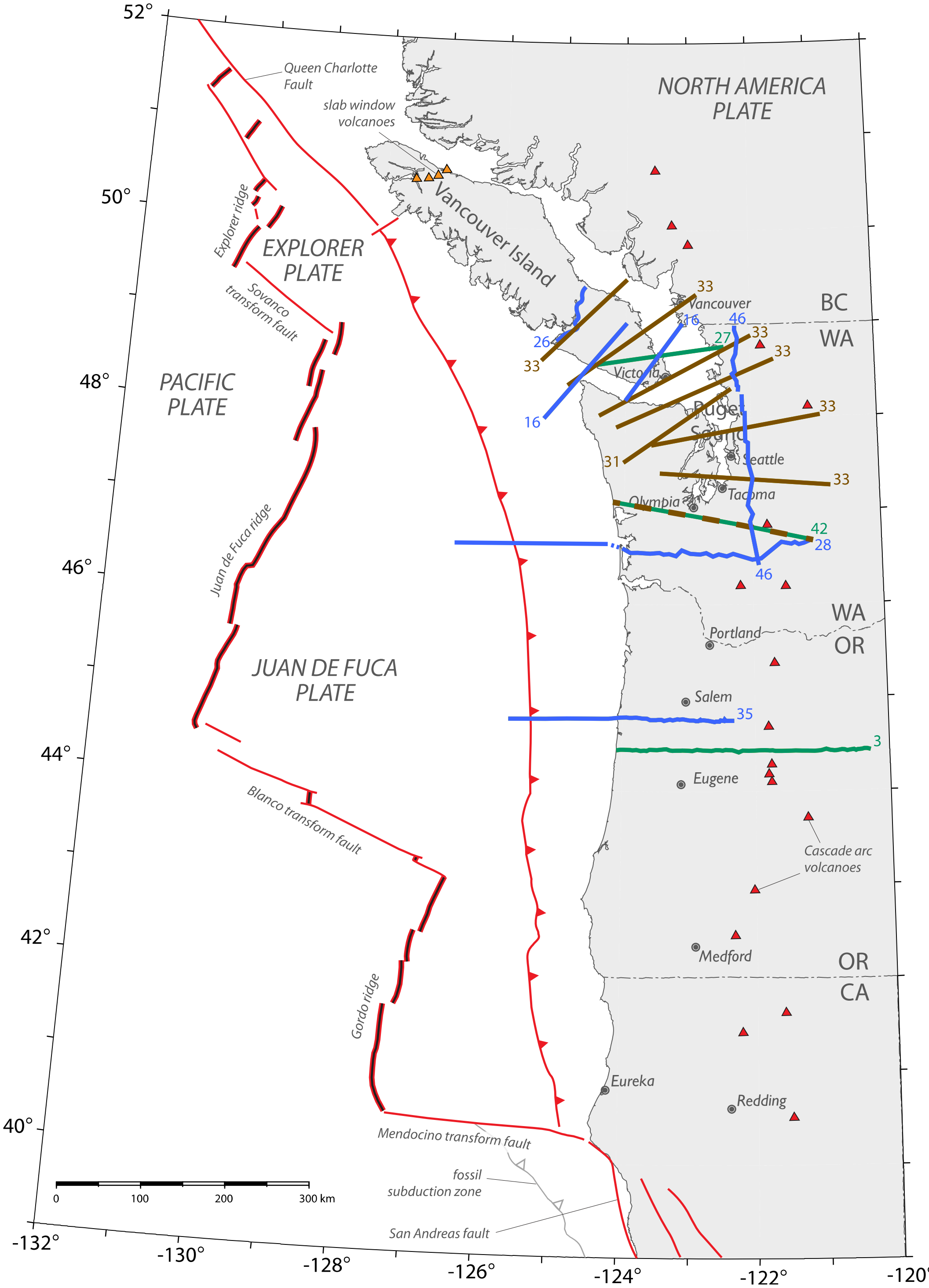

Figure 2. Map showing seismic velocity profiles used to define location of FMC. Numbers refer to references listed in Table 2. Blue lines denote Vp profiles derived from active source experiments; brown lines denote Vp profiles derived from 3-D tomographic models; green lines denote dVs/Vs profiles derived from teleseismic arrays. Note, both Vp and dVs/Vs data are available for the Calvert et al. [2011] profile (labeled 42).

tomographic inversion of seismic refraction and earthquake travel times) depicts a 2–8 km thick Moho layer (Vp 7.3–7.4 km/s) above the fore-arc mantle (Vp 7.6–7.8 km/s) rather than as a sharp Vp discontinuity (Table 2). Miller et al. [1997] interpreted the Moho layer to represent interlayered mafic and ultramafic rocks.

Table 2. Seismic Structure Models Used to Constrain Location of Intersection Between Juan de Fuca Slab and Cascadia Fore-Arc Moho

	Location	Innermost Fore Arc Mantle Vp (km/s)	Geometry of Intersection	Depth of Intersection (km)
2-D Wide Angle (Active Source) Velocity Models				
Nedimović et al. [2003] 26, G	VI	7.3	horizontal	34–44
Graindorge et al. [2003] 16, F	VI		horizontal	35–44[a]
Miller et al. [1997] 46, F	WA	7.6–7.8[b]	rising	30–35
Parsons et al. [1999, 2005] 28, G	WA	7.8[c]		
Tréhu et al. [1994] 35, W	OR	6.5–7.2	horizontal	38[e]
3-D Tomographic Inversion (Active Source) Velocity Models				
Ramachandran et al. [2006] 33, F	VI + WA	7.2–7.6	falling (35–43 km)	38–44
Preston et al. [2003] 31, W	WA	7.5	falling (35 km)	42
Stanley et al. [1999] 44	WA	7.6–7.8	falling (25–34 km)	32–39[d]
Receiver Function (Passive Source) Impedance Models				
Nicholson et al. [2005] 27, F	VI		rising (37 km)	33
Bostock et al. [2002] 3, F	OR		horizontal	33
Brocher et al. [2003] 4, F	OR		horizontal	33
Integrated 3-D (Active and Passive) Models				
Calvert et al. [2011] 42, G	WA	7.5	horizontal	46 ± 3[f]

[a]Moho depth based on gravity data; Moho may be too deep if mantle wedge is hydrated.
[b]2–8 km thick transitional lowermost crustal layer has Vp = 7.3–7.4 km/s.
[c]5 km thick transitional lowermost crustal layer has Vp = 7.5–7.7 km/s; Moho may rise to a depth of 25 km.
[d]Stanley et al. [1999] interpret seismic layer as ultramafic root of Crescent terrane; more likely represents uppermost fore-arc mantle.
[e]Moho depth at 32 km if it correlates with minimum depth estimate for Siletz terrane; at 38 km if it correlates with base of reflective zone; lowermost Siletz terrane has Vp = 6.5–7.2 km/s.
[f]Moho depth based on dVs/Vs; Moho at 38 km if based on Vp; lowermost crust of northern Crescent fore arc terrane has Vp = 6.8–7.2 km/s; lowermost crust of southern Crescent fore-arc terrane has Vp = 6.4–6.8 km/s; Calvert et al. [2011] interpret low velocity zone as oceanic crust (in vicinity of fore arc Moho) with Vp = 6.2 km/s. Note: Values under "Depth to Intersection" heading are as defined in publications; numbers next to references correspond to reference code in McCrory et al. [2012]; G denotes good constraint, F denotes fair; W denotes weak; VI denotes southern Vancouver Island; WA denotes Washington; OR denotes Oregon.

The second set of Moho depths is derived from Parsons et al. [1999, 2005] who constructed an east-west, 510 km long onshore-offshore profile from a 1995–1996 wide-angle refraction/reflection experiment (SW Washington) south of Puget Sound (Figure 2). Their velocity model was constructed from 3-D tomographic inversion of the 1991, 1995, and 1996 transects as well as the 1998 SHIPS survey and regional earthquakes. Similar to Miller et al. [1997], Parsons et al. imaged a 5 km thick Moho layer (Table 2) with a relatively slow velocity (Vp 7.5–7.7 km/s). Parsons et al. [1999, 2005] placed the Moho at the top of this layer based on its reflection signature, and depicted it rising trenchward from ~35 to 30 km.

Only one wide-angle refraction/reflection study is available to constrain the FMC beneath Oregon. Tréhu et al. [1994] constructed an east-west 275 km long profile across central Oregon (Figure 2) based on seismic velocity data collected in 1984 (COCORP), 1989, 1991, and 1993–1994 (IRIS PASSCAL) active and passive source experiments. The fore-arc in central Oregon is composed of thick Siletz oceanic terrane. The base of the terrane is not well resolved because it generates relatively high velocities (Vp 6.5–7.2 km/s) at a relatively shallow depth [Tréhu et al., 1994]. Tréhu et al. [1994] offered a range in Moho depths (Table 2), from 32 km (if the Moho correlates to minimum Siletz thickness) to 38 km (if it correlates to the projected base of a reflective zone). We tentatively favor the deeper estimate because of the similarity in seismic signature between the Oregon reflective zone and the E seismic layer that Nedimović et al. [2003] imaged beneath Vancouver Island.

3.2. Determination of Moho Depth From 3-D Tomographic Inversions

We also constrain the FMC under southern Vancouver Island and the Puget Sound region using three tomographic models constructed from multiple active source experiments. Tomographic models interpolate seismic velocities between data points to fill a 3-D volume, thus tend to blur seismic structures. For our purposes, we assume 2–4 km vertical blurring of key features such as the fore-arc Moho and Juan de Fuca crust.

The first set of Moho depths is derived from Ramachandran et al. [2006] who constructed a regional 3-D Vp tomographic model from the onshore 1991 (Western Cascades) survey and the 1998 (SHIPS) onshore-offshore survey, based on inversion of travel times from active source and earthquake data recorded on temporary arrays and permanent seismographic stations. Ramachandran et al. [2006] modeled the fore-arc upper mantle with an unusually low velocity (Vp 7.2–7.6 km/s) (Table 2). They depicted the Moho as slightly deepening westward on a series of six 150–200 km long slices across southern Vancouver Island and Puget Sound (Figure 2).

Ramachandran et al. [2006] model the FMC as ranging from 38 to 44 km deep on these slices, deeper than most other models. To support a deeper Moho, Ramachandran et al. [2006] suggested that Nedimović et al. [2003]—by placing the top of the Juan de Fuca slab at base of E layer—placed it ~6 km too shallow and that Nicholson et al. [2005]—by misidentifying the top of the E layer as the top of the Juan de Fuca slab (based on teleseismic data discussed below)—placed it ~10 km too shallow. Since the seismic velocity signatures of the E layer and the Juan de Fuca slab are quite similar (i.e., the E layer may represent subducted Paleogene oceanic crust) [McCrory and Wilson, 2013], distinguishing these two seismic structures remains challenging.

Stanley et al. [1999] constructed a tomographic model of western Washington based solely on first-arrivals of regional earthquakes. They interpreted a deep high velocity structure (Vp 7.6–7.8 km/s) as an ultramafic wedge representing a remnant of Crescent mantle. The top of the ultramafic wedge intersects the Juan de Fuca slab at ~32 km in an east-west slice across the Straits of Juan de Fuca region, deepening to 35–39 km in slices across the central and southern Puget Sound region. If we reinterpret the structure as a thick Moho layer (see discussion above), the FMC would be at depths of 32–39 km, similar to the Parsons et al. [1999, 2005] model. We do not incorporate the Stanley et al. [1999] data points into our compilation, however, because of the ambiguity in what their structure represents. Furthermore, this tomographic model has generally been superseded by post-SHIPS models that incorporate active source data. Nonetheless, we cannot rule out the possibility that the high velocity layer beneath Crescent crust may represent residual Crescent mantle material just above where the actual fore-arc Moho is situated, complicating efforts to accurately identify the fore-arc Moho.

The second set of Moho depths is derived from Preston et al. [2003] who constructed a tomographic model for the eastern Olympic Peninsula based on local earthquakes and active source data obtained in four surveys (1991 Western Cascade; 1995–1996 SW Washington; 1998 Wet SHIPS and 1999 Dry SHIPS experiments) by simultaneous inversion of travel times for refracted waves and wide-angle reflected waves. In a NE-trending, 150 km long slice (Figure 2) through the center of their 3-D tomographic model, they depicted the fore-arc Moho as dropping from 35 to 42 km as it approaches the Juan de Fuca plate from the east. Preston et al. [2003] placed the Moho at the 7.5 km/s velocity contour (Table 2), with mantle velocity decreasing to ~7.0 km/s near the FMC.

The third set of Moho depths is derived from Calvert at al. [2011] who constructed a tomographic model of southernmost Vancouver Island and western Washington based on inversion of local earthquakes and active source data from the same four surveys as Preston et al. [2003], plus seismic velocity data from a more recent passive array (CAFE, Cascadia Arrays for Earthscope) deployed in 2006–2008. The Calvert et al. model provides the most comprehensive analysis of seismic structures to date beneath western Washington. Their ESE-trending, 200 km long dVs/Vs profile along the CAFE teleseismic transect across southwestern Washington (Figure 2) images a horizontal Moho at 46 ± 3 km with a fore-arc mantle Vp of 7.5 km/s (Table 2). Calvert at al. [2011] depicted the base of the E layer as situated ~8 km above the Juan de Fuca Moho, consistent with the interpretation of Nedimović et al. [2003] beneath Vancouver Island rather than Ramachandran et al. [2006].

3.3. Determination of Moho Depth From Teleseismic Receiver Function Arrays

We obtain additional FMC depth constraints between southern Vancouver Island and central Oregon using three seismic impedance models. Profiles of Vs perturbations (dVs/Vs) from receiver function analyses typically image the Moho beneath the Cascade Arc as a reversal from relatively slow lower crust to fast upper mantle [e.g., Bostock et al., 2002]. This velocity contrast weakens trenchward, and the polarity typically reverses where slab depths are shallower than 40 km [Bostock et al., 2002].

The first set of Moho depths is derived from Nicholson et al. [2005] who constructed a dVs/Vs profile across Vancouver Island from a 2002–2004 (Polaris) passive experiment based on scattered wave inversions. The Moho boundary is sharp to east and becomes more subdued as it approaches slab to the west. Nicholson et al. [2005] placed the FMC at 33 km (Table 2) in their NE-trending, 250 km long transect (Figure 2), rising from 37 to 38 km further east. The second set of depths, derived

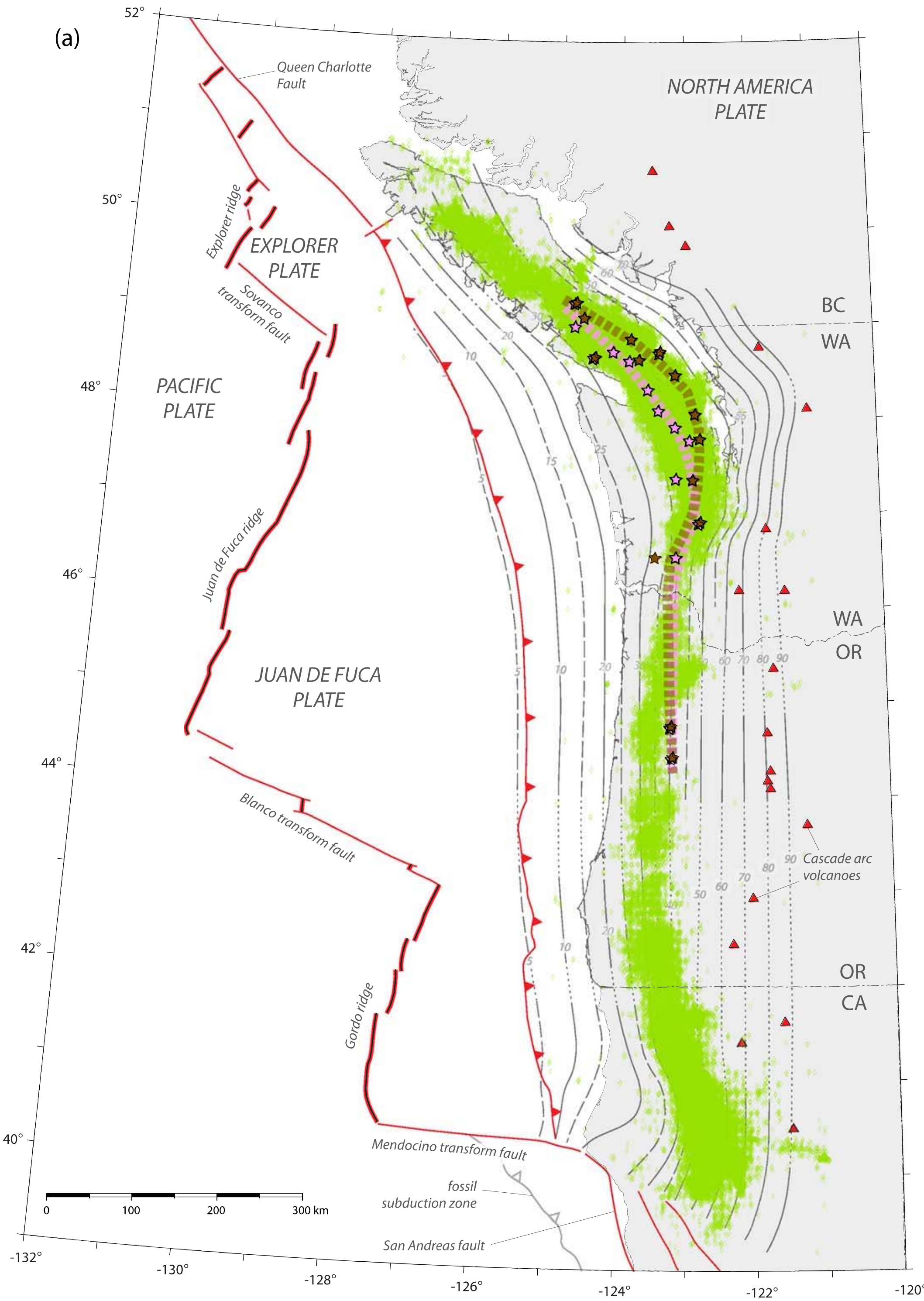

Figure 3. Maps showing location of FMC based on seismic velocity profiles, tremor, and the Juan de Fuca slab surface. (a) Control points, denoted by brown stars, and FMC, denoted by dashed brown line, are based on geographic (Option XY-A) constraints in the original publications. Control points, denoted by magenta stars, and FMC, denoted by dashed magenta line, use horizontal datums for all profiles (Option XY-H). (See Figure 1 for explanation of other symbols.) (b) Control points, denoted by brown stars, and FMC, denoted by dashed brown line, are based on depth (Option Z-A) constraints in the original publications. Control points, denoted by magenta stars, and FMC, denoted by dashed magenta line, use horizontal datums for all profiles (Option Z-H). (See Figure 1 for explanation of other symbols.)

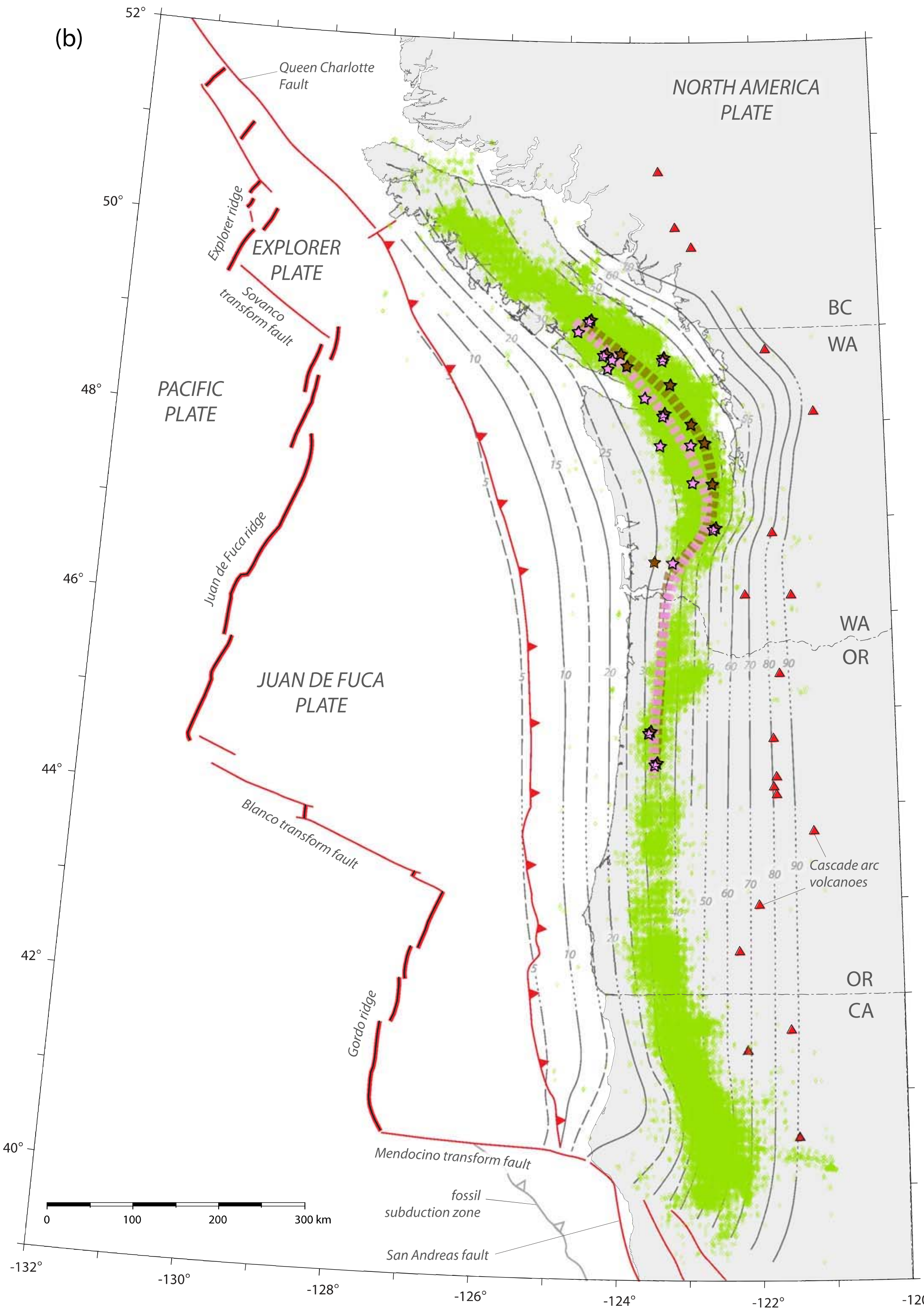

Figure 3. Continued

from Calvert et al. [2011] dVs/Vs profiles across southernmost Vancouver Island and western Washington, is discussed above.

The third set of Moho depths is derived from Bostock et al. [2002] who constructed a dVs/Vs profile beneath central Oregon from the 1993–1994 (IRIS PASSCAL) teleseismic experiment, based on forward and backward scattered P- to S-wave conversions. Bostock et al. placed a horizontal fore-arc Moho at a depth of ∼34 km

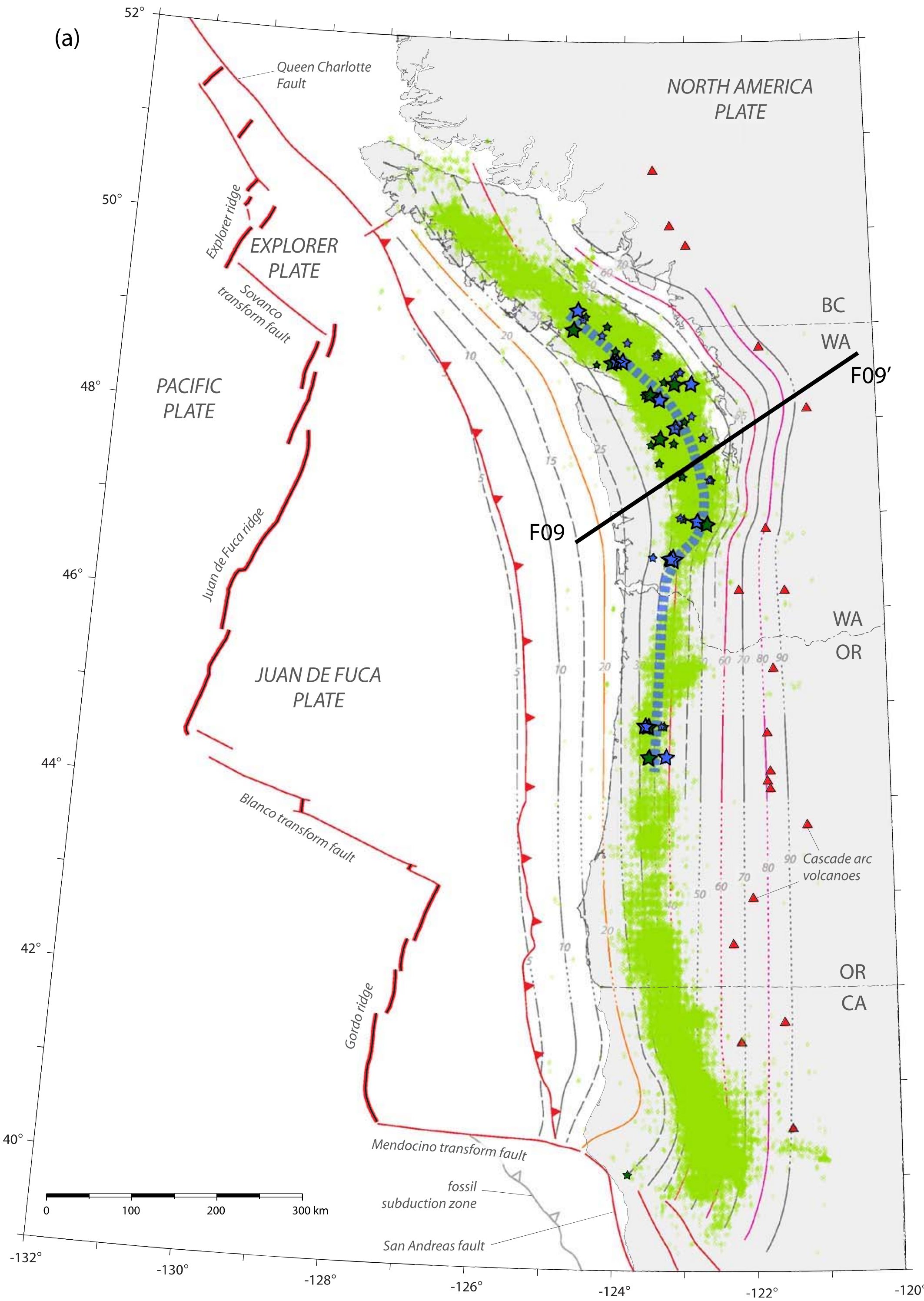

Figure 4. (a) Map showing location of FMC based on seismic velocity profiles, tremor, and the Juan de Fuca slab surface. Slab depth contours in 20 km increments colored to be consistent with Figures 5a and 6a. Best-fit FMC contour, denoted by blue dashed line, green stars denote locations based on geographic constraints (Option XY); blue stars denote locations based on depth constraints (Option Z); smaller stars denote weak constraints (see Table 2); bigger stars denote fair or good constraints. Heavy black line denotes location of profile shown in Figure 4b. Note that the updip limit of tremor roughly correlates with location of green (XY) control points. (See Figure 1 for explanation of other symbols.) (b) Generalized profile showing location of thermally inferred locked zones from Hyndman and Rogers [2010], tremor band (note, tremor depths not constrained), and fore-arc Moho. (See Figure 4a for profile location.) Juan de Fuca slab crust denoted by thick gray line; tremor denoted by green diamonds; ANSS hypocenters from McCrory et al. [2012] denoted by black dots. Inverted brown triangle marks trench axis; inverted blue triangle marks coastline; red triangle marks Cascade volcanic arc. (c) Map showing tremor density over a two year period intended to capture all segments of ETS along the subduction margin given their ~11.5–21.5 month recurrence intervals [Holtkamp and Brudzinski, 2010]. (See Figure S5 for distribution of seismograph stations recording tremor.) Best-fit FMC contour denoted by black dashed line.

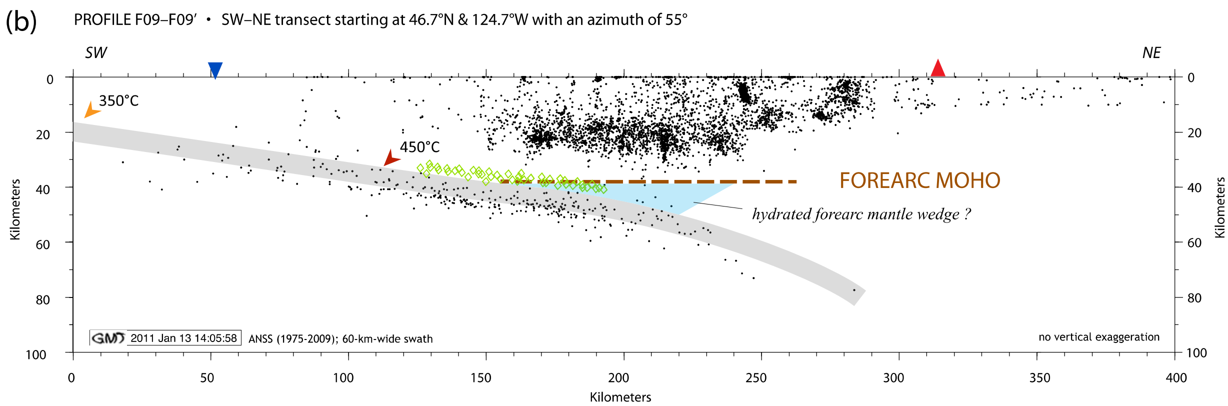

Figure 4. Continued

(Table 2) on their east-west 300 km long profile across central Oregon (Figure 2). Their depth estimate is within the 32–38 km range indicated by Trehu et al. [1994].

4. Locating the Fore-Arc Mantle Corner and the Updip Extent of Tremor

Seismic structure models are inherently nonunique as they require trade-offs between the velocity and thickness of seismic layers encountered within the subduction margin. Faster assigned velocities result in apparently deeper structures and vice versa. In addition, the difficulties in delineating the location of the FMC owing to the lack of sharp contrasts in Vp, Vs, and dVs/Vs data are illustrated by the range of Moho geometries depicted in the seismic structure models discussed above. Most of the models depict the Moho as a nearly horizontal velocity discontinuity, a few depict it as a seaward rising discontinuity and even fewer depict it as a seaward dropping discontinuity (Table 2).

We construct four versions of the intersection. Option XY-A depicts a geographical location (i.e., latitude and longitude) of the FMC obtained from map views of the published profiles (supporting information, Figure S1). Option Z-A depicts the depths obtained from the profiles, but shifted as needed to where those depths intersect the McCrory et al. [2012] slab model (Figure S2). Option XY-H (Figure S3) and (4) Option Z-H (Figure S4) employ horizontal datums only. For these versions, we extrapolate a horizontal Moho for datums that have been depicted as rising or dropping—from where the datums are well imaged in the fore-arc region—and combine these locations with those which had been depicted as horizontal originally.

Given the uncertainties in estimating depths for lower crustal reflectors and refractors, the vertical blurring of tomographic structures, and the inherent low resolution of Vs perturbations, we favor published geographic locations over Moho depths depicted in the profiles. Even so, the geographic location of the FMC comes with significant uncertainty. For example, Parsons et al. [2005] considered their 3-D velocity model to have lateral uncertainties of ± 15–20 km at a depth (22 km) considerably shallower than the Moho. Given the lack of robust constraints on the Moho geometry near the corner, we also favor using horizontal datums—extrapolated and original—for Moho depth (Option H) as this option offers a consistent data set.

Using the geographical (Option XY-A) method, we construct an intersection that ranges from 35 to 45 km deep (Figure 3a). For this version, the intersection is about 40 km deep beneath Vancouver Island, 45 km beneath Strait of Georgia and Puget Sound, and 40 km again beneath southern Washington into central Oregon. Since most dipping datums depict a seaward dropping Moho (Table 2), restricting the data set to horizontal Moho data points (Option XY-H) yields a slightly tighter and shallower range, from 38 to 42 km deep, shifting the FMC about 25 km westward relative to the deeper datum (Figure 3a).

Using the depth (Option Z-A) method yields an intersection about 38 km deep in the north, 43 km beneath Puget Sound, then abruptly rising to 30 km from southern Washington into central Oregon (Figure 3b). Using only horizontal Moho data points (Option Z-H), again yields a slightly tighter and shallower range, about 35 km deep beneath southern Vancouver Island, 40 km beneath the Olympic Peninsula, and 35 km

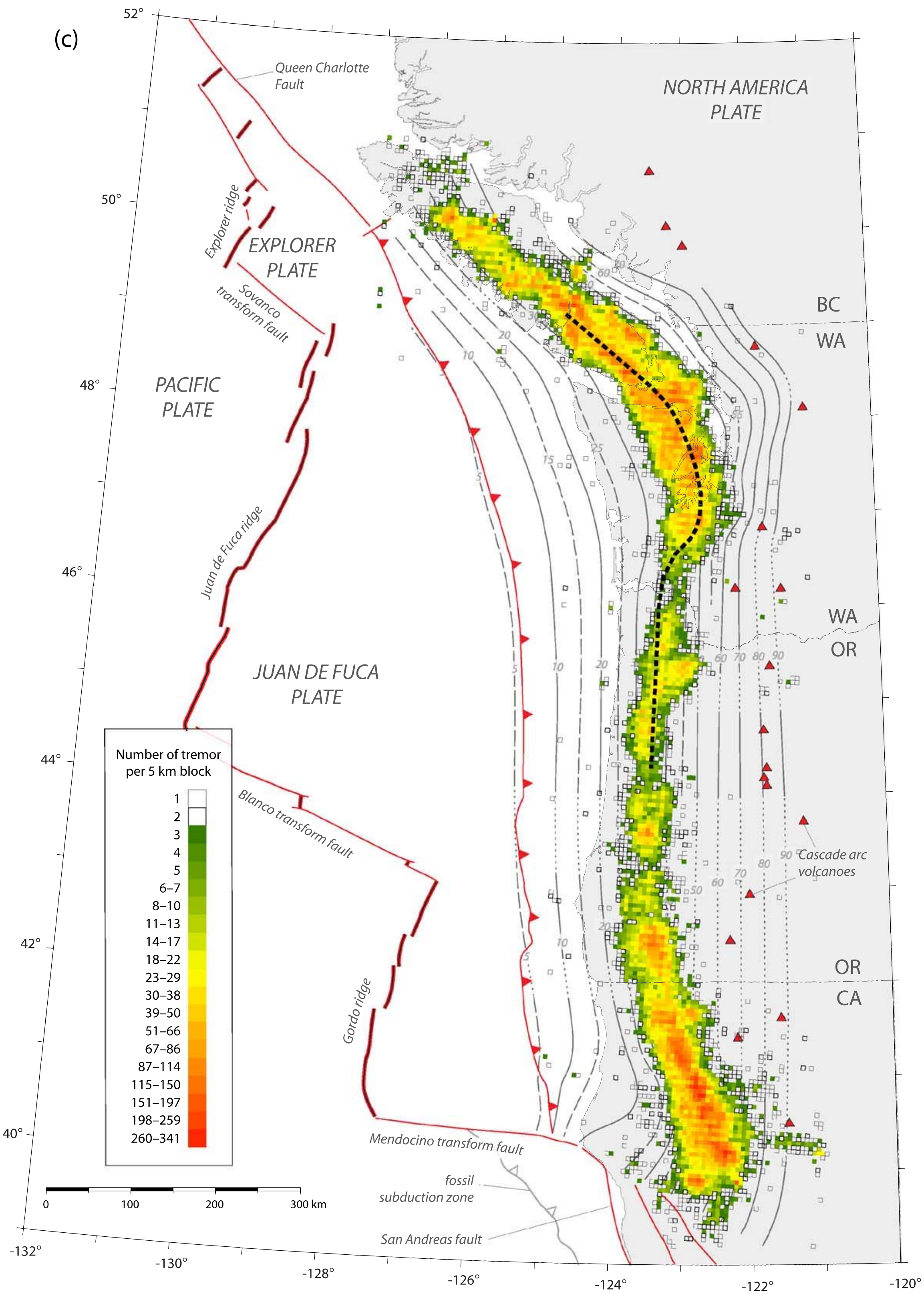

Figure 4. Continued

(a)

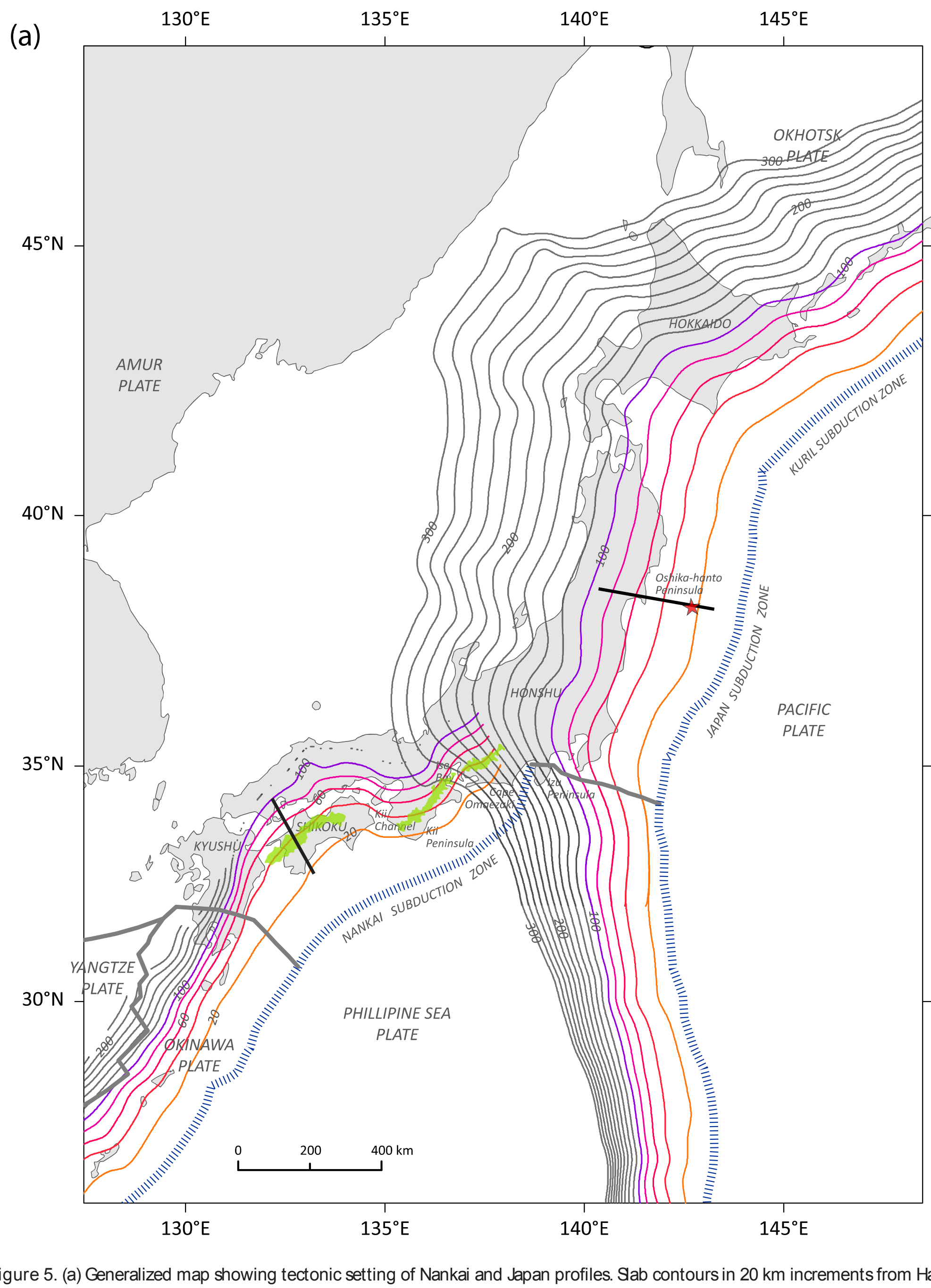

Figure 5. (a) Generalized map showing tectonic setting of Nankai and Japan profiles. Slab contours in 20 km increments from Hayes et al. [2012] with contours down to 100 km colored for clarity; tectonic boundaries from Bird [2003] with dashed blue lines denoting subduction boundaries; tremor from Shelly et al. [2006] denoted in green pattern. Red star marks epicenter of 2011 Tohoku earthquake. Heavy black lines denote location of profiles shown in Figures 5b and 5c. (b) Generalized profile across the Nankai subduction zone (modified from profile A of Shelly et al. [2006]) showing location of thermally inferred locked zones, tremor band (note, tremor depths not constrained), and fore-arc Moho. Philippine Sea slab crust denoted by thick gray line; inverted blue triangles mark coastlines for the islands of Honshu and Shikoku. (See Figure 4b for description of other symbols.) (c) Generalized profile across the Japan subduction zone in vicinity of 2011 Tohoku earthquake (modified from profile c-c' of Yamamoto et al. [2011]) showing location of thermally inferred locked zones, dry fore-arc mantle wedge, and fore-arc Moho. Pacific slab crust denoted by thick gray line; hypocenters denoted by black dots; red star marks projected location of Tohoku hypocenter; other symbols as in Nankai profile. (See Table 1 for sources of various parameters for both profiles.)

again beneath central Oregon (Figure 3b). In summary, under southern Vancouver Island and Washington, the intersection—as defined by horizontal datums (Option H)—is about 5 km shallower than an intersection defined by dipping datums (Option A) for both the XY and Z methods.

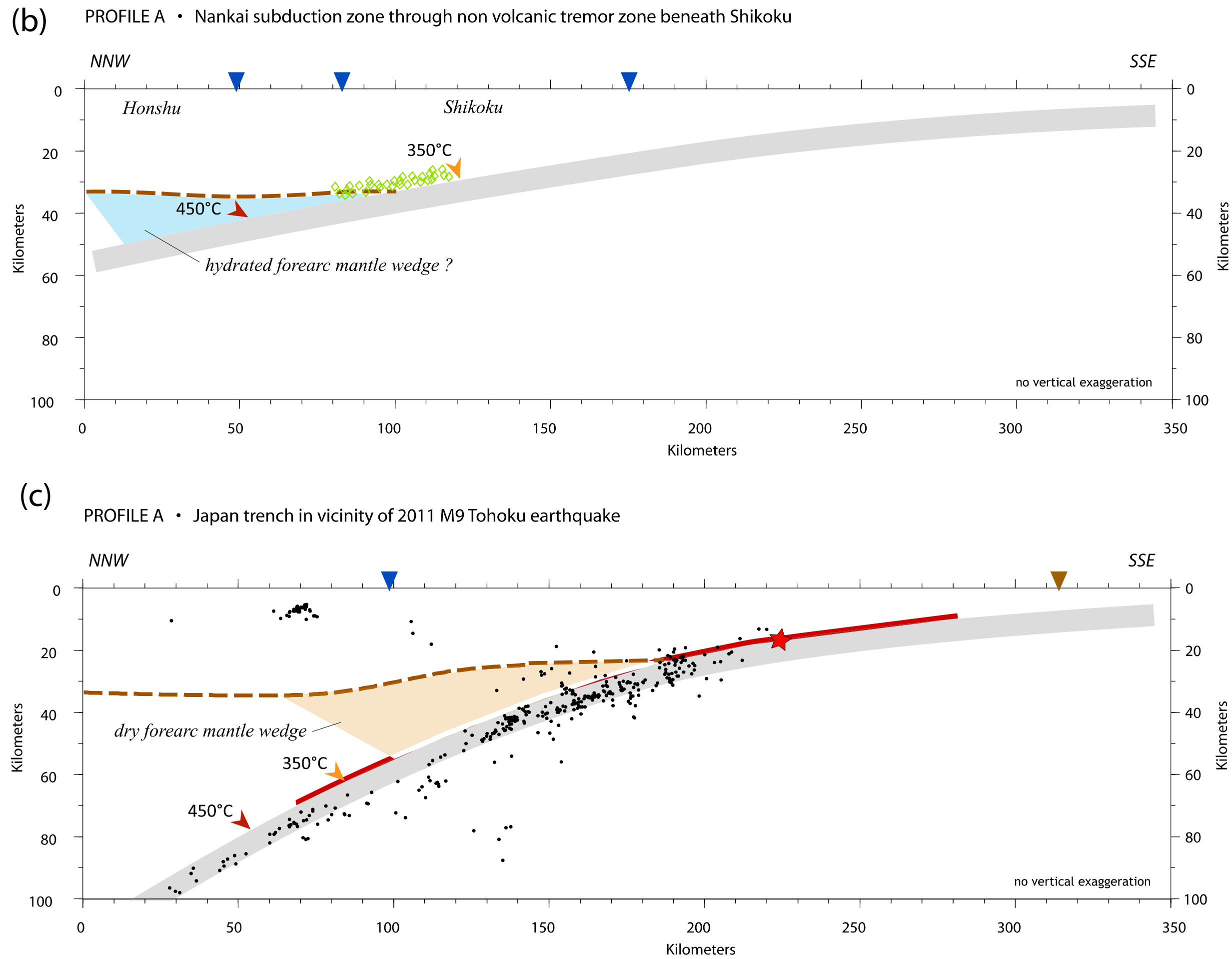

Figure 5. Continued

Finally, we derive a "best estimate" curve for the location of the FMC from a synthesis of these four permutations. The better constrained depths (Table 2) indicate an intersection 36–38 km deep beneath southern Vancouver Island, 41–43 km deep beneath Washington, and 35–40 km deep beneath Oregon (Figure 4a). Thus the best constrained data depict the same general pattern, with a somewhat shallower intersection beneath Vancouver Island and northern Oregon than beneath Washington. All permutations indicate a marked westward shift in the FMC south of about 47°N, consistent with the abrupt shift to a steeper slab dip.

Our compilation illustrates considerable scatter in depth estimates (Figures 3, 4a, and S1–S4), even though many publications incorporated much of the same velocity data in their models. Some variability can be attributed to the velocities assigned to fore-arc mantle (ranging from 7.2 to 7.8 km/s; Table 2). The scatter also reflects the difficulty in identifying the Moho discontinuity as it transitions from a well-defined discontinuity near the volcanic arc [e.g., Brocher et al., 2003, Figure 2] to an often poorly resolved one near the FMC.

We plot the distribution of almost 100,000 tremor "epicenters" based on two years of data (Figures 1, 3, and 4) extracted from A. Wech's database (http://www.pnsn.org/tremor; 1 January 2012–1 January 2014). These tremor concentrate in a band which extends from northern Vancouver Island to northern California. The detection threshold appears fairly uniform along the subduction margin based on the distribution of seismograph stations recording tremor (Figure S5). Epicentral uncertainties for the tremor are less than 5 km [Wech and Creager, 2008; Wech, 2010]. Tremor appears to be located near or somewhat above the subduction interface although depths are not well constrained, so are not considered further.

An envelope defined by the updip and downdip extent of NVT curves in concert with slab geometry. Envelope width is narrower where the slab dips more steeply and wider where the slab dips less steeply. All FMC data points—regardless of plotting method—locate within the tremor envelope (Figures 3 and 4a). The XY-H intersection generally plots within the middle of the envelope, implying that tremor extends both updip and downdip from the FMC. The Z-H intersection generally plots near the updip edge of tremor, implying that tremor is restricted to the innermost mantle wedge.

Overall uncertainty in the location of the intersection precludes resolving which correlation is more reliable. Nonetheless, the FMC data provide a striking consistency with the shape of the tremor band. Where the intersection appears to be relatively shallow—tremor overlies relatively shallow slab (Figure 4a), and conversely where the intersection appears to be relatively deep—tremor overlies relatively deep slab. These observations imply that the spatial distribution of NVT is not defined by slab depth, rather correlates to the location of the FMC. If tremor signals high pore fluid pressure, then the distribution of tremor should reflect the presence of fluids at these depths and perhaps the existence of permeability barriers that confine fluids in this region. Interestingly, our best-fit curve falls along the zone of most abundant tremor within the tremor band (Figure 4c), suggesting a concentration of high fluid pressure along the FMC.

5. Comparisons to Other Subduction Zones

The Cascadia fore-arc mantle wedge appears to be hydrated, consistent with the predicted release of geo-fluids from oceanic crust beneath the fore-arc mantle wedge in warm subduction zones. In cool subduction zones, where most geo-fluids are released well downdip from the FMC, the innermost mantle wedge appears to be dry. Such dry mantle wedges are associated with the Japan and Sumatra subduction systems [e.g., Dessa et al., 2009; Yamamoto et al., 2011] where recent great earthquakes have ruptured past the fore-arc Moho into the mantle wedge. Thus discerning whether or not the innermost mantle wedge is hydrated, or more specifically, whether stable sliding minerals are present along the subduction fault, is key to determining whether the FMC could control the extreme downdip limit of seismogenic slip.

5.1. Seismogenic Role of the FMC in Nankai Subduction System

The Nankai subduction zone along southwestern Japan offers a well studied analog for the Cascadia subduction system since it is also characterized as a warm subduction system [Kodaira et al., 2002] (Table 1). The subducting Philippine Sea plate arches beneath Shikoku and buckles beneath the Kii Peninsula (Figure 5). The plate contains the Kyushu-Palau volcanic ridge subducting beneath Kyushu and the Izu-Bonin volcanic ridge subducting beneath Ise Bay. These features result in a strongly heterogeneous subduction interface which is reflected in the variability in locking depths, from 20 to 40 km, along the subduction margin [Wallace et al., 2012]. Juan de Fuca plate geometry is complex as well, with a tight arch beneath northern California and a broader arch beneath Washington plus isolated subducting seamounts [e.g., Tréhu et al., 2012]. Fault locking appears to extend somewhat deeper in the arched portion beneath Washington (Figure 1) [McCaffrey et al., 2013].

Most of the Nankai fore-arc mantle appears to contain 15–25% serpentine from the Moho down to where the slab reaches a depth of ~50 km [Seno, 2005; Xia et al., 2008; Matsubara et al., 2009]. Where the slab is strongly warped beneath eastern Shikoku–Kii Channel and Ise Bay [Hirose et al., 2008], however, relatively low Vp/Vs values in the mantle [Matsubara et al., 2009] suggest little serpentinization, raising the question of whether the deeper locked zone beneath Shikoku reflects dry mantle conditions. Similar Vp/Vs data are not available to determine the hydration state above the arched sections of the Juan de Fuca plate.

The Nankai fore-arc Moho, at a depth of ~25–30 km (arched Shikoku segment) [e.g., Obara, 2002; Kodaira et al., 2002], is significantly shallower than the 34–43 km depths we map for Cascadia. Conversely, thermal models predict significantly deeper temperature thresholds for the Nankai subduction interface, reaching 350°C at a slab depth of ~28 km and 450°C at ~42 km [Seno, 2005] compared to Cascadia depths of ~13 km and ~27 km, respectively (Table 1). The 1944 Mw8.1 Tonankai earthquake ruptured down to slab depths of 23–25 km [Nakanishi et al., 2002], well short of the downdip end of the geodetically defined locked zone beneath Shikoku, yet in the vicinity of both its FMC and the 350°C thermal front. These observations do not allow us to distinguish whether the FMC or the 350°C threshold exerted the overriding control on rupture depth. For Cascadia, with a shallower 350°C threshold and a deeper FMC, these features are widely separated, potentially providing an opportunity to evaluate their relative significance.

Cascadia and Nankai are the only subduction systems with well documented temporal and spatial correlations between episodic tremor and slow slip. Nankai tremor occurs within a 35–50 km wide zone above slab depths of 30–35 km (just below the downdip end of to the locked zone) from the eastern end of Kyushu to Tokai (Figure 5), with persistent gaps in tremor activity in the vicinity of Kii Channel and Ise Bay [Obara, 2002; Ito et al., 2007; Hirose et al., 2008; Brown et al., 2009] where the slab appears strongly warped [Hirose et al., 2008] and serpentinization of the fore-arc mantle minimal [Matsubara et al., 2009]. These depths are similar to those observed in Cascadia, moreover, tremor beneath Shikoku is situated just downdip from the FMC, broadly comparable to our observations for Cascadia (Figure 4a). The abundance and recurrence rate of tremor also vary along the Cascadia subduction margin [Holtkamp and Brudzinski, 2010], with minor persistent gaps beneath the Columbia River and Eugene, Oregon (Figure 4c). In contrast to Nankai, the most abundant Cascadia tremor occurs where the slab is warped (Figure 4c). We do not know the degree of serpentinization above the warped Juan de Fuca plate beneath northern California.

Tremor beneath Shikoku (arched segment) occurs where thermal models predict a slab temperature of $425 \pm 50^\circ$C, whereas deeper tremor beneath the Kii Peninsula (buckled segment) occurs where models predict a lower temperature of $325 \pm 50^\circ$C [Peacock, 2009]. Beneath Vancouver Island, tremor occurs where a much higher temperature of $575 \pm 50^\circ$C is predicted [Peacock, 2009]. This variability suggests that tremor does not mark equivalent metamorphic conditions [Hyndman and Wang, 1995; Peacock, 2009]. In the Shikoku region, for example, Fagereng and Diener [2011] suggested that temperatures and pressures associated with the tremor band correlate with the release of fluids associated with dehydration of lawsonite whereas in the much warmer Vancouver Island region, tremor correlates with dehydration of chlorite and glaucophane. This inherent variability cautions against simple extrapolations between Nankai and Cascadia. Furthermore, Cascadia tremor occurs well downdip from the locked zone and the 350°C threshold, unlike Nankai which does not exhibit a gap between the downdip limit of its locked zone and the updip limit of tremor.

For much of the Nankai subduction zone, the FMC, the 350°C threshold, the downdip limit of the locked zone, and the updip limit of NVT broadly overlap at a slab depth of ~30 km (Table 1). The locked zone beneath Shikoku as defined by Wallace et al. [2012] may extend past the Moho intersection down to a depth near the 450°C threshold, however, coseismic rupture during instrumentally recorded great earthquakes did not extend past the 350°C threshold nor into hydrated fore-arc mantle. These observations suggest the potential for coseismic rupture to extend past the Moho where the fore-arc mantle wedge is not serpentinized, but we have no direct evidence that this has occurred in the past. In summary, since the potential constraints we would like to evaluate, namely the FMC and the updip limit of NVT, occur at comparable depths to thermal and geodetic constraints, Nankai provides little insight into whether either feature might control of the downdip limit of coseismic rupture.

5.2. Seismogenic Role of FMC During the 2011 Mw9.0 Tohoku-Oki Earthquake

The Japan subduction zone off northern Honshu and Hokkaido is characterized as a cool subduction system [Nakanishi et al., 1989] (Table 1). The Pacific plate is broadly buckled at its northern end beneath Hokkaido [Hayes et al., 2012] where the subduction zone changes orientation to become the Kuril-Kamchatka subduction system (Figure 5). Seamounts subducting offshore from Ibaraki Prefecture, result in a somewhat heterogeneous subduction interface [Mochizuki et al., 2008].

The 2011 Mw9.0 Tohoku earthquake ruptured the central portion of the Japan subduction zone, adjacent to the Fukushima, Miyagi, and Iwate prefectures [Romano et al., 2012], from near the trench down to where the Pacific slab is 60–70 km deep beneath the coastline [Romano et al., 2012]. Geodetic observations suggest strong locking on the subduction interface adjacent to the Miyagi (central segment) and Aomori (northern segment) prefectures [Suwa et al., 2006; Yamamoto et al., 2011] down to 60–70 km, well below the Japan FMC at a depth of ~20 km, [e.g., Takahashi et al., 2000; Hino et al., 2000; Ito et al., 2005]. The strongly locked regions are characterized by dry, stagnant mantle (i.e., isolated from convective flow) down to a slab depth of ~60 km based on heat flow values and detailed 3-D seismic tomography [Yamamoto et al., 2011]. In fact, the 2011 hypocenter and maximum fault slip occurred off the Oshika-hanto Peninsula (near Sendai), where high Vp (8.0 km/s) implies little serpentinization of the mantle situated between the FMC and the coastline. Rather than the FMC providing a limit to coseismic rupture, the limit coincides with the intersection between the slab and a velocity discontinuity in the fore-arc mantle wedge that appears to mark the updip limit to corner flow of hydrated mantle [Yamamoto et al., 2011].

10.1002/2013GC005144

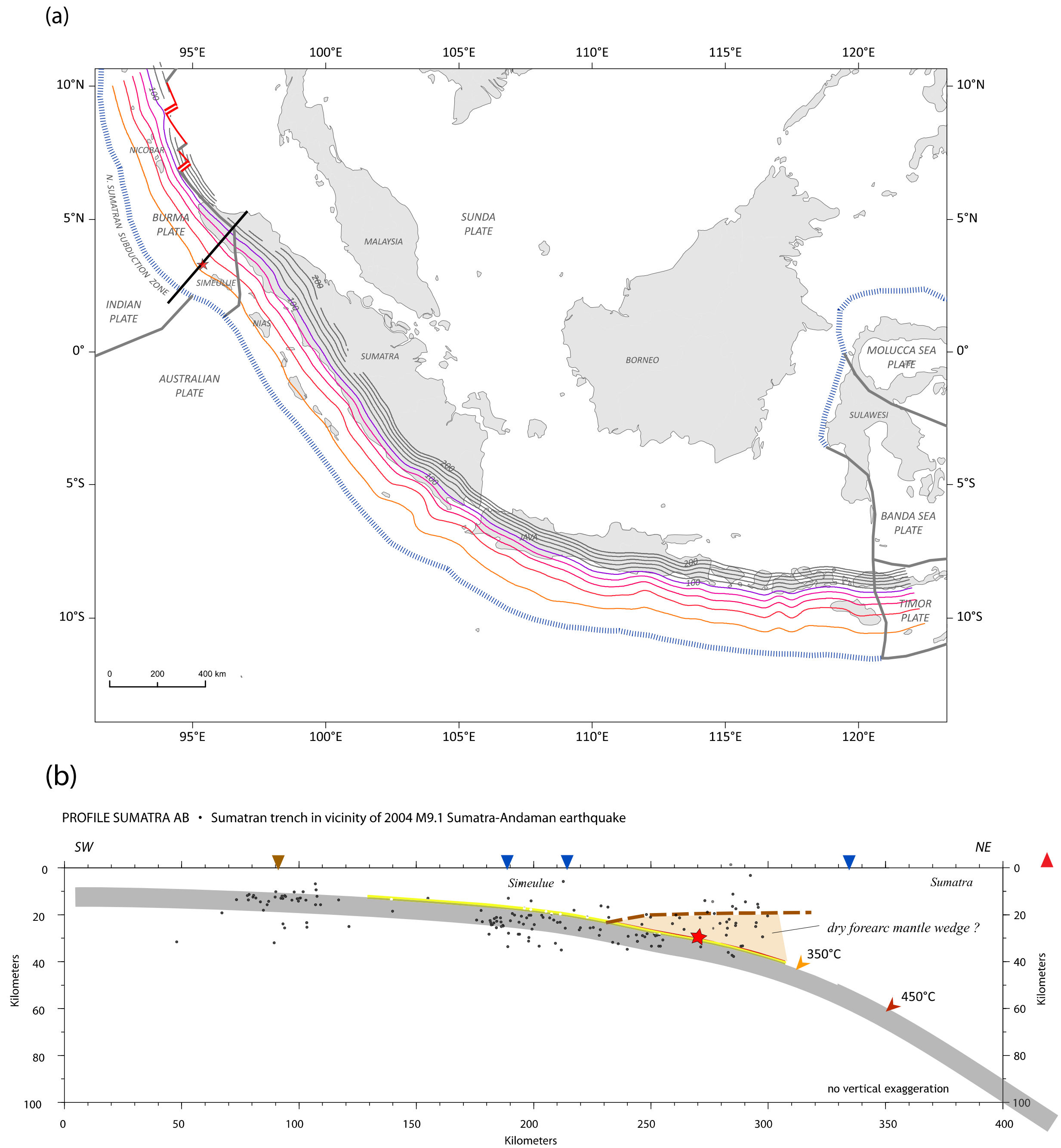

Figure 6. (a) Generalized map showing tectonic setting of the Sumatra profile. Slab contours in 20 km increments from Hayes et al. [2012] with contours down to 100 km colored for clarity; tectonic boundaries from Bird [2003] with dashed blue line denoting subduction boundaries. Red star marks epicenter of 2004 Andaman-Sumatra earthquake. Heavy black line denotes location of profile shown in Figure 6b. (b) Generalized profile across northern Sumatra subduction zone in vicinity of Andaman-Sumatra earthquake (modified from Klingelhoefer et al. [2010, Figure 9]) showing location of thermally inferred locked zones and fore-arc Moho. Indo-Australian slab crust denoted by thick gray line; red star marks hypocenter of 2004 Andaman-Sumatra earthquake. Inverted blue triangles mark coastlines for the islands of Simeulue and Sumatra. (See Figure 4b for description of other symbols. See Table 1 for sources of various parameters.)

Instrumentally recorded earthquakes on the Japan subduction fault much smaller than the Tohoku event have also ruptured past the FMC. The 1994 Mw 7.7 Sanriku-Oki earthquake offshore northernmost Honshu ruptured down to a slab depth of ∼50 km, with maximum fault slip (∼5 m) occurring deeper than the FMC [Hino et al., 2000]. Similarly, 1978 Mw 7.5 Miyagi-Oki subduction earthquake offshore northern Honshu ruptured down to a depth of ∼60 km [Seno, 2005]. Thermal models predict that the Pacific plate crust reaches a temperature of 350°C at about 63 km depth, and 450°C at about 78 km depth [Peacock, 2003], both well below the fore-arc Moho (Table 1). Thus, the downdip rupture extent for these earthquakes is consistent with a geodetic constraint, a 350°C thermal constraint, and a hydrated mantle constraint, but not a FMC constraint.

In summary, high resolution seismic tomography in the vicinity of the Tohoku earthquake [Yamamoto et al., 2011] provides evidence that hydration state of the fore-arc mantle wedge may play a significant role in limiting both the extent of coseismic rupture as well as the amount of slip. Since the depths of the geodetic and thermal constraints broadly overlap with the shift from relatively dry to wet mantle conditions, we are unable to isolate their roles in controlling downdip rupture.

5.3. Seismogenic Role of the FMC During the 2004 Mw9.1 Sumatra-Andaman Earthquake

The Sumatran subduction zone is characterized as a cool subduction system with the subducting Indo-Australian plate ranging in age from 45 to 60 Ma at the trench [Dessa et al., 2009]. The Indo-Australian plate is broadly arched near the northern tip of Sumatra (Figure 6) [Hayes et al., 2012], and contains a volcanic ridge that is subducting beneath Simeulue Island [Klingelhoefer et al., 2010]. The Andaman Islands to the north have sparse GPS data, so little is known about the spatial extent of the locked zone in the vicinity of the 2004 Mw 9.1 Sumatra-Andaman earthquake from geodetic observations. Thermal modeling predicts that the seismogenic zone extends down to a slab depth of ~40 km [Hippchen and Hyndman, 2008; Klingelhoefer et al., 2010]. Immediately to the south, in the Simeulue Island region, the locked zone extends down to a slab depth of ~50 km [Prawirodirdjo et al., 1997; McCaffery, 2009] based on limited GPS observations. Currently neither the seismograph network nor the GPS network are sufficient to detect whether or not NVT or SSE, respectively, occur along the Sumatra subduction margin.

The Sumatra FMC is quite shallow, ~21 to 25 km deep (curving downward as it approaches the slab) [Dessa et al., 2009; Klingelhoefer et al., 2010]. Thermal modeling predicts a temperature of 350°C at a slab depth of ~37 km and 450°C at ~57 km [Hippchen and Hyndman, 2008; Klingelhoefer et al., 2010], both much deeper than the FMC (Table 1). The 2004 Mw 9.1 earthquake ruptured from Simeulue Island ~1500 km northward past the Andaman Islands [McCaffrey, 2009]. Rupture initiated at a depth of 32 ± 3 km [Dessa et al., 2009], well below the inferred FMC, yet near the 350°C threshold [Klingelhoefer et al., 2010].

A tomographic velocity model in the vicinity of the 2004 Mw9.1 hypocenter, based on a 2006 active source experiment, yielded a Vp of 8.0 km/s for the mantle wedge down to a slab depth of at least 30 km (deepest extent of velocity model), implying little serpentinization of the innermost mantle wedge [Klingelhoefer et al., 2010]. Thus, the 2004 earthquake appears to provide another example of great earthquake rupture extending past the fore-arc Moho in subduction settings where the innermost mantle wedge is not significantly hydrated. The 2005 Mw8.6 Nias-Simeulue earthquake to the south also ruptured past the fore-arc Moho and the geodetically inferred locked zone [Briggs et al., 2006; McCaffrey, 2009].

In summary, comparison of Nankai, Japan, and Sumatra subduction systems with the Cascadia subduction zone emphasizes the importance of plate age or more specifically, its thermal state, in controlling the downdip extent of coseismic rupture by modulating the depth of brittle-to-ductile mineral transformations and the depth of mineral dehydration processes. Of course, dehydration of oceanic crust can only occur if it became hydrated while it transits from the spreading ridge to the trench. Owing to the extreme young age of the Juan de Fuca plate and the existence highly fractured propagator wakes within the plate, some studies predict considerable variability in its hydration state [e.g., Nedimović et al., 2009; Cozzens and Spinelli, 2012], in apparent contradiction to evidence for widespread hydrated mantle discussed above. For subduction zones where fore-arc mantle hydration occurs well downdip from the FMC, we are able to ascertain the importance of hydration—or more specifically the presence of stable sliding minerals along the subduction interface—in limiting coseismic rupture. The generally accepted correlation between high fluid pore pressures and tremor occurrence underscore the importance of elucidating both thermal state and hydration state of a subduction system when evaluating coseismic rupture limits.

6. Implications for Mode of Slip in the Cascadia Gap Zone

Available evidence from subduction zones in Japan and Indonesia underlines the importance of mantle hydration in limiting downdip coseismic rupture and the degree to which hydration state can vary within systems based on the temperature (i.e., age) and geometry of the incoming oceanic plate. This variability, along with permeability conditions, results in significant heterogeneity with respect to frictional properties along the subduction fault by perturbing pore fluid pressures, the depth of brittle-to-ductile mineral transitions, and the presence or absence of stable sliding minerals.

For Cascadia, the release of geo-fluids derived from dehydration of oceanic crust is expected to occur beneath both fore-arc crust and mantle based on thermal and rheologic models [e.g., Peacock, 2009]. Heat flow observations from southern Vancouver Island suggest that the mantle wedge above a slab depth of 50 km is stagnant [Peacock, 2009]. A weak Moho signature beneath Washington and southern British Columbia suggests widespread serpentinized fore-arc mantle [Bostock et al., 2002; Brocher et al., 2003]. High Poisson's ratios in the fore-arc mantle beneath southern Vancouver Island (~0.28) [Ramachandran and Hyndman, 2012] also support an interpretation of significant serpentinization. Neither Vp/Vs nor Poisson's ratio values, however, are available to extend this interpretation further south along the Cascadia margin. Nonetheless, we infer hydrated conditions based on the similarity in seismic velocity structures along the margin which denote anomalously low mantle velocities [e.g., Brocher et al., 2003], and thereby assume great earthquakes will not rupture past the FMC.

Unlike Nankai, Japan, and Sumatra, the Cascadia FMC is located much deeper than the downdip limit of the geodetically inferred locked zone and the 350°C threshold (Table 1). So we turn to the question of how plate convergence is accommodated in the ~70 km wide gap between the downdip end of the locked zone at a slab depth of ~ 20–25 km and the FMC at ~38–42 km, or more narrowly, the ~50 km wide gap between the downdip edge of the locked zone and the updip edge of the tremor band at ~35 km depth. We cannot yet ascertain the favored modes of slip within this gap zone. Nor have we fully documented the favored modes of slip in the ETS zone. Ten years of GPS observations suggest that SSE account for up to 65% of relative plate motion on the subduction interface at a slab depth of ~35 km [Schmidt and Gao, 2010]. The remaining plate motion is likely accommodated by currently undetected aseismic slip between SSE, aseismic slip following coseismic rupture, or both.

If a currently undetected slip deficit extends into the gap zone, it would represent a potentially damaging source of ground shaking relatively close to major population centers. Seismic hazard assessments currently model this gap zone as weakly seismogenic and the tremor zone as freely slipping [e.g., Petersen et al., 2008]. Other modes of slip behavior, however, might reasonably be expected. We suggest four end members for seismogenic behavior within the gap. The first two have implications for hazard estimates by potentially affecting the probability of great earthquake occurrence; the last one has major implications for coseismic hazard.

1. The gap region creeps continuously. This end member would require that slip is currently not well resolved by geodetic observations, and that no detectable tremor accompanies creep. This case would tend to damp the influence of deep SSE in promoting great earthquakes.

2. The gap region is currently locked, but slips in slow events with long, as yet unobserved, recurrence times or will slip as the currently detected deeper SSE move progressively updip with time. As with option (1), this end member would require that current estimates of locking depth are not resolving the behavior in this region (in this case not resolving a lack of slip). Any future slip in the gap (occurring either eventually or episodically) would increase the probability of great earthquake occurrence.

3. The gap region slips as after-slip or during aftershocks following a great earthquake. This end member implies that the geodetic estimates of locking depth are adequate, and has no implications for great earthquake occurrence.

4. The gap region is currently locked, and slips coseismically during great earthquake ruptures. This end member is currently evaluated in seismic hazard assessments [e.g., Petersen et al., 2008] and would significantly increase the coseismic hazard of great earthquakes by increasing rupture area beyond geodetic and thermal rupture models.

7. Summary

We examine the FMC and the updip limit of ETS as possible controls on downdip rupture limit for great earthquakes on the Cascadia subduction fault. Both of these features are situated downdip from the rupture limit predicted by geodetic and thermal models, leaving a gap up to 70 km wide where the mode of slip remains unresolved. Nonetheless, we can reasonably assume that the FMC and ETS serve as the extreme lower bounds on rupture during great earthquakes, based on seismic velocity evidence that the fore-arc mantle wedge is significantly serpentinized. Resolving possible heterogeneity in the degree of serpentinization along the Cascadia subduction margin will require comprehensive, higher resolution 3-D seismic velocity and thermal models than are currently available. In the interim, the presence of tremor provides indirect evidence of hydrated conditions.

Our analysis suggests that the fore-arc Moho corner is shallower along the northern Cascadia segment beneath southern Vancouver Island (36–38 km) and the central segment beneath Oregon (35–40 km), than along the intervening segment beneath Washington (41–43 km). We lack the data needed to determine Moho depth for the southern Cascadia segment beneath northern California. Owing to the difficulty in accurately determining Moho depths where there is weak seismic velocity contrast between fore-arc lower crust and mantle, this variation in depth requires additional data and a uniform modeling approach for confirmation.

As in Nankai, the distribution of Cascadia tremor correlates with the fore-arc mantle corner. This relationship may be fortuitous, if geo-fluids that we assume promote tremor are coincidentally released from Juan de Fuca crust near the mantle corner. The detection of tremor well updip from the FMC in other warm subduction settings such as Central America cautions against prematurely interpreting a causal relationship. Additional heat flow and seismic velocity studies that allow inferences about dehydration/hydration processes and pathways and barriers for geo-fluids are needed to better delineate the extreme downdip limit of seismogenic rupture. Meanwhile, the range in character among subduction zones around the Pacific Rim offers natural laboratories for deducing key parameters and isolating their role in limiting downdip rupture during great earthquakes.

Acknowledgments
We thank Nick Beeler, Art Frankel, Diane Moore, Jack Boatwright, and two anonymous reviewers for constructive comments which improved this contribution.

References

Abers G. A., L. S. MacKenzie, S. Rondenay, Z. Zhang, A. G. Wech, and K. C. Creager (2009), Imaging the source region of Cascadia tremor and intermediate-depth earthquakes, Geology, 29(12), 1119–1122, doi:10.1130/G30143A.1.

Atwater, B. F., et al. (1995), Summary of coastal geologic evidence for past great earthquakes at the Cascadia subduction zone, Earthquake Spectra, 11(1), 1–18.

Bartlow, N. M., S. Miyazaki, A. M. Bradley, and P. Segall (2011), Space-time correlation of slip and tremor during the 2009 Cascadia slow slip event, Geophys. Res. Lett., 38, L18309, doi:10.1029/2011GL048714.

Bird, P. (2003), An updated digital model of plate boundaries, Geochem. Geophys. Geosyst., 4(3), 1027, doi:10.1029/2001GC000252.

Blanpied, M. L., D. A. Lockner, and J. D. Byerlee (1991), Fault stability inferred from granite sliding experiments at hydrothermal conditions, Geophys. Res. Lett., 18, 609–612.

Blanpied, M. L., D. A. Lockner, and J. D. Byerlee (1995), Frictional slip of granite at hydrothermal conditions, J. Geophys. Res., 100, 13,045–13,064.

Bostock, M. G., R. D. Hyndman, S. Rondenay, and S. M. Peacock (2002), An inverted continental Moho and serpentinization of the forearc mantle, Nature, 417, 536–538.

Boyarko, D. C., and M. R. Brudzinski (2010), Spatial and temporal patterns of nonvolcanic tremor along the southern Cascadia subduction zone, J. Geophys. Res., 115, B00A22, doi:10.1029/2008JB006064.

Briggs R. W., et al. (2006), Deformation and slip along the Sunda megathrust in the great 2005 Nias-Simeulue earthquake, Science, 311, 1897–1901, doi:10.1126/science.1122602.

Brocher, T. M., T. Parsons, A. M. Tréhu, C. M. Snelson, and M. A. Fisher (2003), Seismic evidence for widespread serpentinized forearc upper mantle along the Cascadia margin, Geology, 31(3), 267–270.

Brown, J. R., G. C. Beroza, S. Ide, K. Ohta, D. R. Shelly, S. Y. Schwartz, W. Rabbel, M. Thorwart, and H. Kao (2009), Deep low-frequency earthquakes in tremor localize to the plate interface in multiple subduction zones, Geophys. Res. Lett., 36, L19306, doi:10.1029/2009GL040027.

Calvert, A. J., L. A. Preston, and A. M. Farahbod (2011), Sedimentary underplating at the Cascadia mantle-wedge corner revealed by seismic imaging, Nat. Geosci., 4, 545–548, doi:10.1038/NGEO1195.

Chapman, J. S., and T. I. Melbourne (2009), Future Cascadia megathrust rupture delineated by episodic tremor and slip, Geophys. Res. Lett., 36, L22301, doi:10.1029/2009GL040465.

Christensen, N. I. (1966), Elasticity of ultrabasic rocks, J. Geophys. Res., 71, 5921–5931.

Christensen, N. I. (1996), Poisson's ratio and crustal seismology, J. Geophys. Res., 101, 3139–3156.

Christensen, N. I. (2004), Serpentinites, peridotites, and seismology, Int. Geol. Rev., 46, 795–816.

Christensen, N. I. and W. D. Mooney (1995), Seismic velocity structure and composition of the continental crust: A global view, J. Geophys. Res., 100, 9761–9788, doi:10.1029/95JB00259.

Cozzens, B. D., and G. A. Spinelli (2012), A wider seismogenic zone at Cascadia due to fluid circulation in subducting oceanic crust, Geology, 40(10), 899–902, doi:10.1130/G33019.1.

Delouis, B., J.-M. Nocquet, and M. Vallée (2010), Slip distribution of the February 27, 2010 Mw = 8.8 Maule Earthquake, central Chile, from static and high-rate GPS, InSAR, and broadband teleseismic data, Geophys. Res. Lett., 37, L17305, doi:10.1029/2010GL043899.

Dessa J.-X., F. Klingelhoefer, D. Graindorge, C. André, H. Permana, M.-A. Gutscher, A. Chauhan, S. C. Singh, and the SUMATRA-OBS Scientific Team (2009), Megathrust earthquakes can nucleate in the forearc mantle: Evidence from the 2004 Sumatra event, Geology, 37(7), 659–662, doi:10.1130/G25653A.1.

Doğan, T., J. Sumino, K. Nagao, K. Noesu (2006), Release of mantle helium from forearc region of the Southwest Japan arc, Chem. Geol., 233, 235–248.
Fagereng, Å., and J. F. A. Diener (2011), Non-volcanic tremor and discontinuous slab dehydration, Geophys. Res. Lett., 38, L15302, doi:10.1029/2011GL048214.
Flück, P., R. D. Hyndman, and K. Wang (1997), Three-dimensional dislocation for great earthquakes of the Cascadia subduction zone, J. Geophys. Res., 102, 20,539–20,550.
Graindorge, D., G. Spence, P. Charvis, J. Y. Collet, R. D. Hyndman, and A. M. Tréhu (2003), Crustal structure beneath the Strait of Juan de Fuca and southern Vancouver Island from seismic and gravity analyses, J. Geophys. Res., 108(B10), 2484, doi:10.1029/2002JB001823.
Hawkes A. D., B. P. Horton, A. R. Nelson, C. H. Vane, and Y. Sawai (2011), Coastal subsidence in Oregon, USA, during the giant Cascadia earthquake of AD 1700, Quat. Sci. Rev., 30, 364–376, doi:10.1016/j.quascirev.2010.11.017.
Hayes, G. P., D. J. Wald, and R. L. Johnson (2012), Slab 1.0: A three-dimensional model of global subduction zone geometries, J. Geophys. Res., 117, B01302, doi:10.1029/2011JB008524.
He, C., L. Luo, Q.-M. Hao, and Y. Zhou (2013), Velocity-weakening behavior of plagioclase and pyroxene gouges and stabilizing effect of small amounts of quartz under hydrothermal conditions, J. Geophys. Res. Solid Earth, 118, 3408–3430, doi:10.1002/jgrb.50280.
Hino, R., S. Ito, H. Shioara, H. Shimamura, T. Sato, T. Kanazawa, J. Kasahara, and A. Hasegawa (2000), Aftershock distribution of the 1994 Sanriku-oki earthquake (Mw 7.7) revealed by ocean bottom seismographic observation, J. Geophys. Res., 105, 21,697–21,710.
Hippchen, S., and R.D. Hyndman (2008), Thermal and structural models of the Sumatra subduction zone: Implications for the megathrust seismogenic zone, J. Geophys. Res., 113, B12103, doi:10.1029/2008JB005698.
Hirose, F., J. Nakajima, and A. Hasegawa (2008), Three-dimensional seismic velocity structure and configuration of the Philippine Sea slab in southwestern Japan estimated by double-difference tomography, J. Geophys. Res., 113, B09315, doi:10.1029/2007JB005274.
Holtkamp, S., and M. R. Brudzinski (2010), Determination of slow slip episodes and strain accumulation along the Cascadia margin, J. Geophys. Res., 115, B00A17, doi:10.1029/2008JB006058.
Hyndman, R. D. (2004), Controls on subduction thrust earthquakes: Down-Dip changes in composition and state, in Rheology and Deformation of the Lithosphere at Continental Margins, edited by G. D. Karner, Karner et al., 166–178, Columbia Univ. Press, New York.
Hyndman, R. D. (2013), Downdip landward limit of Cascadia great earthquake rupture, J. Geophys. Res. Solid Earth, 118, 5530–5549, doi:10.1002/jgrb.50390.
Hyndman, R. D., and K. Wang (1993), Thermal constraints on the zone of major thrust earthquake failure: The Cascadia Subduction Zone, J. Geophys. Res., 98, 2039–2060, doi:10.1029/92JB02279.
Hyndman, R. D., and K. Wang (1995), The rupture zone of Cascadia great earthquakes from current deformation and the thermal regime, J. Geophys. Res., 100, 2133–22,154.
Hyndman, R. D., and G. C. Rogers (2010), Great earthquakes on Canada's west coast: A review, Can. J. Earth Sci., 47, 801–820, doi:10.1139/E10–011.
Hyndman, R. D., M. Yamano, and D. A. Oleskevich (1997), The seismogenic zone of subduction thrust faults, Island Arc, 6, 244–260, doi:10.1111/j.1440-1738.1997.tb00175.x.
Ide, S., D. R. Shelly, and G. C. Beroza (2007), Mechanism of deep low frequency earthquakes: Further evidence that deep non-volcanic tremor is generated by shear slip on the plate interface, Geophys. Res. Lett., 34, L03308, doi:10.1029/2006GL028890.
Ito, A., G. Fujie, S. Miura, S. Kodaira, R. Hino, and Y. Kaneda (2005), Bending of the subducting oceanic plate and its implication for rupture propagation of large interplate earthquakes off Miyagi, Japan, in the Japan trench subduction zone, Geophys. Res. Lett., 32, L05310, doi:10.1029/2004GL022307.
Ito, Y., K. Obara, K. Shiomi, S. Sekine, and H. Hirose (2007), Slow earthquakes coincident with episodic tremors and slow slip events, Science, 315(26), 503–506, doi:10.1126/science.1134454.
Kelsey, H. M., A. R. Nelson, E. Hemphill-Haley, and R. C. Witter (2005), Tsunami history of an Oregon coastal lake reveals a 4600 yr record of great earthquakes on the Cascadia subduction zone, Geol. Soc. Am. Bull., 117(7-8), 1009–1032.
Klingelhoefer, F., M.-A. Gutscher, S. Ladage, J.-X. Dessa, D. Graindorge, D. Franke, C. Andre, H. Permana, T. Yudistira, and A. Chauhan (2010), Limits of the seismogenic zone in the epicentral region of the 26 December 2004 great Sumatra-Andaman earthquake: Results from seismic refraction and wide-angle reflection surveys and thermal modeling, J. Geophys. Res., 115, B01304, doi:10.1029/2009JB006569.
Kodaira, S., E. Kurashimo, J.-O. Park, N. Takahashi, A. Nakanishi, S. Miura, T. Iwasaki, N. Hirata, K. Ito, and Y. Kaneda (2002), Structural factors controlling the rupture process of a megathrust earthquake at the Nankai trough seismogenic zone, Geophys. J. Int., 149, 815–835.
Kostoglodov, V., A. Husker, N. M. Shapiro, J. S. Payero, M. Campillo, N. Cotte, and R. Clayton (2010), The 2006 slow slip event and non volcanic tremor in the Mexican subduction zone, Geophys. Res. Lett., 37, L24301, doi:10.1029/2010GL045424.
La Rocca, M., K. C. Creager, D. Galluzzo, S. Malone, J. E. Vidale, J. R. Sweet, and A. G. Wech (2009), Cascadia tremor located near plate interface constrained by S minus P wave times, Science, 323, 620–623, doi:10.1126/science.1167112.
La Rocca, M., D. Galluzzo, S. Malone, W. McCausland, and E. Del Pezzo (2010), Array analysis and precise source location of deep tremor in Cascadia, J. Geophys. Res., 115, B00A20, doi:10.1029/2008JB006041.
Leonard, L. J., R. D. Hyndman, and S. Mazzotti (2004), Coseismic subsidence in the 1700 great Cascadia earthquake: Coastal estimates versus elastic dislocation models, Geol. Soc. Am. Bull., 116(5–6), 655–670, doi:10.1130/B25369.1.
Leonard, L. J., C. A. Currie, S. Mazzotti, and R. D. Hyndman (2010), Rupture area and displacement of past Cascadia great earthquakes from coastal coseismic subsidence, Geol. Soc. Am. Bull., 122(11–12), 2079–2096, doi:10.1130/B30108.1.
Loveless, J. P., and B. J. Meade (2011), Spatial correlation of interseismic coupling and coseismic rupture extent of the 2011 MW 5 9.0 Tohoku-oki earthquake, Geophys. Res. Lett., 38, L17306, doi:10.1029/2011GL048561.
Matsubara, M., K. Obara, and K. Kasahara (2009), High-Vp/Vs zone accompanying non-volcanic tremors and slow-slip events beneath southwestern Japan, Tectonophysics, 472, 6–17.
McCaffrey, R. (1997), Influences of recurrence times and fault zone temperatures on the age-rate dependence of subduction zone seismicity, J. Geophys. Res., 102, 22,839–22,854.
McCaffrey, R. (2009), The tectonic framework of the Sumatran subduction zone, Annu. Rev. Earth Planet. Sci., 37, 345–366, doi:10.1146/annurev.earth.031208.100212.
McCaffrey, R., R. W. King, S. J. Payne, and M. Lancaster (2013), Active tectonics of northwestern U.S. inferred from GPS-derived surface velocities, J. Geophys. Res. Solid Earth, 118, 709–723, doi:10.1029/2012JB009473.
McCrory, P. A. (2000), Upper plate contraction north of the migrating Mendocino triple junction, northern California: Implications for partitioning of strain, Tectonics, 19, 1144–1160.
McCrory, P. A., and D. S. Wilson (2013), A kinematic model for the formation of the Siletz-Crescent terrane by capture of coherent fragments of the Farallon and Resurrection plates, Tectonics, 32, 718–736, doi:10.1002/tect.20045.

McCrory, P. A., J. L. Blair, F. Waldhauser, and D. H. Oppenheimer (2012), Juan de Fuca slab geometry and its relation to Wadati-Benioff zone seismicity, J. Geophys. Res., 117, B09306, doi:10.1029/2012JB009407.
Miller, K. C., G. R Keller, J. M. Gridley, J. H. Luetgert, W. D. Mooney, and H. Thybo (1997), Crustal structure along the west flank of the Cascades, western Washington, J. Geophys. Res., 102, 17,857–17,873.
Mochizuki, K., T. Yamada, M. Shinohara, Y. Yamanaka, and T. Kanazawa (2008), Weak interplate coupling by seamounts and repeating M □ 7 earthquakes, Science, 321, 1194–1197, doi:10.1126/science.1160250.
Moore, D. E., and D. A. Lockner (2007), Comparative deformation behavior of minerals in serpentinized ultramafic rock: Application to the slab-mantle interface in subduction zones, Int. Geol. Rev., 49, 401–415.
Moore, D. E., and D. A. Lockner (2008), Talc friction in the temperature range 25°–400°C: Relevance for fault-zone weakening, Tectonophysics, 449, 120–132.
Moore, D. E., D. A. Lockner, S. Ma, R. Summers, J. D. Byerlee (1997), Strengths of serpentinite gouges at elevated temperatures, J. Geophys. Res., 102, 14,787–14,801.
Moreno, M., et al. (2011), Heterogeneous plate locking in the South–Central Chile subduction zone: Building up the next great earthquake, Earth Planet. Sci. Lett., 305, 413–424, doi:10.1016/j.epsl.2011.03.025.
Nakanishi, A., N. Takahashi, J.-O. Park, S. Miura, S. Kodaira, Y. Kaneda, N. Hirata, T. Iwasaki, and M. Nakamura (2002), Crustal structure across the coseismic rupture zone of the 1944 Tonankai earthquake, the central Nankai trough seismogenic zone, J. Geophys. Res., 107(B1), EPM 2-1–EPM 2–21, doi:10.1029/2001JB000424.
Nakanishi, M., K. Tamaki, and K. Kobayashi (1989), Mesozoic magnetic anomaly lineations and seafloor spreading history of the Northwestern Pacific, J. Geophys. Res., 94, 15,437–15,462.
Nedimović, M. R., R. D. Hyndman, K. Ramachandran, and G. D. Spence (2003), Reflection signature of seismic and aseismic slip on the northern Cascadia subduction interface, Nature, 424, 416–420, doi:10.1038/nature01840.
Nedimović, M. R., D. R., Bohnenstiehl, S. M. Carbotte, J. P. Canales, R. P. Dziak (2009), Faulting and hydration of the Juan de Fuca plate system, Earth Planet. Sci. Lett., 284, 94–102, doi:10.1016/j.epsl.2009.04.013.
Nicholson T., M. Bostockand J. F. Cassidy (2005), New constraints on subduction zone structure in northern Cascadia, Geophys. J. Int., 161, 849–859, doi:10.1111/j.1365-246X.2005.02605.x.
Obara, K. (2002), Non-volcanic deep tremor associated with subduction in southwest Japan, Science, 296, 1679–1681, doi:10.1126/science.1070378.
Obara, K. (2009), Inhomogeneous distribution of deep slow earthquake activity along the strike of the subducting Philippine Sea Plate, Gondwana Res., 16, 512–526, doi:10.1016/j.gr.2009.04.011.
Obara, K., H. Hirose, F. Yamamizu, and K. Kasahara (2004), Episodic slow slip events accompanied by non-volcanic tremors in southwest Japan subduction zone, Geophys. Res. Lett., 31, L23602, doi:10.1029/2004GL020848.
Obermeier, S. F. (1995), Preliminary estimates of the strength of prehistoric shaking in the Columbia River valley and the southern half of coastal Washington, with emphasis for a Cascadia subduction zone earthquake about 300 years ago, U.S. Geol. Surv. Open-File Rep., 94–589, 46 p.
Oleskevich D. A., R. D. Hyndman, K. Wang (1999), The updip and downdip limits to great subduction earthquakes: Thermal and structural models of Cascadia, south Alaska, SW Japan, and Chile, J. Geophys. Res., 104, 14965–14991, doi:10.1029/1999JB900060.
Parsons, T., R. E. Wells, and M. A. Fisher (1999), Three-dimensional velocity structure of Siletzia and other accreted terranes in the Cascadia forearc of Washington, J. Geophys. Res., 104, 18,015–18,039.
Parsons, T., et al. (2005), Crustal structure of the Cascadia fore arc of Washington, U.S. Geol. Surv. Prof. Pap., 1661-D, 45 p.
Peacock, S. M. (2003), Thermal structure and metamorphic evolution of subducting slabs. in Inside the Subduction Factory, Geophys. Monogr. 138, edited by J. Eiler, pp. 7–22, AGU, Washington, D. C.
Peacock, S. M. (2009), Thermal and metamorphic environment of subduction zone episodic tremor and slip, J. Geophys. Res., 114, B00A07, doi:10.1029/2008JB005978.
Peacock, S. M., and R. D. Hyndman (1999), Hydrous minerals in the mantle wedge and the maximum depth of subduction thrust earthquakes, Geophys. Res. Lett., 26, 2517–2520.
Peacock, S. M., K. Wang, and A. M. McMahon (2002), Thermal structure and metamorphism of subducting oceanic crust—Insight into Cascadia intraslab earthquakes, U.S. Geol. Surv. Open-File Rep., 02–328, 123–126.
Peacock S. M., N. I. Christensen, M. G. Bostock, and P. Audet (2011), High pore pressures and porosity at 35 km depth in the Cascadia subduction zone, Geology, 39(5), 471–474, doi:10.1130/G31649.1.
Petersen, M. D., et al. (2008), Documentation for the 2008 Update of the United States National Seismic Hazard Maps, U.S. Geol. Surv. Open-File Rep., 2008-1128, 61 p.
Prawirodirdjo, L., Y. Bock, R. McCaffrey, J. Genrich, E. Calais, C. Stevens, S. S. O. Puntodewo, C. Subarya, and J. Rais (1997), Geodetic observations of interseismic strain segmentation at the Sumatra subduction zone, Geophys. Res. Lett., 24, 2601–2604.
Preston, L. A., K. C. Creager, R. S. Crosson, T. M. Brocher, and A. M. Trehu (2003), Intraslab earthquakes: Dehydrating the Cascadia slab, Science, 302, 1197–2000.
Ramachandran, K. (2001), Velocity structure of S.W. British Columbia, and N.W. Washington, from 3-D non-linear seismic tomography, PhD dissertation, 198 pp, Univ. of Victoria, Victoria, B. C.
Ramachandran, K., and R. D. Hyndman (2012), The fate of fluids released from subducting slab in northern Cascadia, Solid Earth, 3, 121–129, doi:10.5194/se-3-121-2012.
Ramachandran, K., R. D. Hyndman, and T. M. Brocher (2006), Regional P wave velocity structure of the northern Cascadia subduction zone, J. Geophys. Res., 111, B12301, doi:10.1029/2005JB004108.
Rogers, G., and H. Dragert (2003), Episodic tremor and slip on the Cascadia subduction zone: The chatter of silent slip, Science, 300(5627), 1942–1943, doi:10.1126/science.1084783.
Romano F., A. Piatanesi, S. Lorito, N. D'Agostino, K. Hirata, S. Atzori, Y. Yamazaki, and M. Cocco (2012), Clues from joint inversion of tsunami and geodetic data of the 2011 Tohoku-oki earthquake, Nature, 2(385), 8, doi:10.1038/srep00385.
Schmidt, D. A., and H. Gao (2010), Source parameters and time-dependent slip distributions of slow slip events on the Cascadia subduction zone from 1998 to 2008, J. Geophys. Res., 115, B00A18, doi:10.1029/2008JB006045.
Scholz, C. H. (1990), The Mechanics of Earthquakes and Faulting, 439 pp., Cambridge Univ. Press, New York.
Schwartz, S. Y., and J. M. Rokosky (2007), Slow slip events and seismic tremor at circum-pacific subduction zones, Rev. Geophys., 45, RG3004, doi:10.1029/2006RG000208.
Seno, T. (2005), Variation of down-dip limit of the seismogenic zone near the Japanese islands: Implications for the serpentinization mechanism of the forearc mantle wedge, Earth Planet. Sci. Lett., 231, 249–262, doi:10.1016/j.epsl.2004.12.027.

Shearer, P., and R. Bürgmann, (2010), Lessons Learned from the 2004 Sumatra-Andaman megathrust rupture, Annu. Rev. Earth Planet. Sci., 38, 103–131, doi:10.1146/annurev earth-040809-152537.
Shelly, D. R., G. C. Beroza, S. Ide, and S. Nakamula (2006), Low-frequency earthquakes in Shikoku, Japan, and their relationship to episodic tremor and slip, Nature, 442, 188–191, doi:10.1038/nature04931.
Simons, M., et al. (2011), The 2011 magnitude 9.0 Tohoku-Oki earthquake: Mosaicking the megathrust from seconds to centuries, Science, 332, 1421–1425, doi:10.1126/science.1206731.
Stanley, W. D., A. Villaseñor, and H. M. Benz (1999), Subduction zone and crustal dynamics of western Washington: A tectonic model for earthquake hazards evaluation, U.S. Geol. Surv. Open-file Rep., 99–311, 66 pp. [Available at: http://pubs.usgs.gov/of/1999/ofr-99–0311/.]
Suwa, Y., S. Miura, A. Hasegawa, T. Sato, and K. Tachibana (2006), Interplate coupling beneath NE Japan inferred from three-dimensional displacement field, J. Geophys. Res., 111, B04402, doi:10.1029/2004JB003203.
Takahashi, N., S. Kodaira, T. Tsuru, J. Park, Y. Kaneda, and H. Kinoshita (2000), Detailed plate boundary structure off northeast Japan coast, Geophys. Res. Lett., 27, 1977–1980, doi:10.1029/2000GL008501.
Tréhu, A. M., I. Asudeh, T. M. Brocher, J. H. Luetgert, W. D. Mooney, J. L. Nabelek, and Y. Nakamura (1994), Crustal architecture of the Cascadia forearc, Science, 266, 237–243.
Tréhu, A. M., R. J. Blakely, and M. C. Williams (2012), Subducted seamounts and recent earthquakes beneath the central Cascadia forearc, Geology, 40, 103–106, doi:10.1130/G32460.1.
Verma, S. P. (2002), Absence of Cocos plate subduction-related basic volcanism in southern Mexico: A unique case on Earth?, Geology, 30(12), 1095–1098.
Wallace, L. M., Å. Fagereng, and S. Ellis (2012), Upper plate tectonic stress state may influence interseismic coupling on subduction megathrusts, Geology, 40(10), 895–898, doi:10.1130/G33373.1.
Wech, A. G. (2010), Interactive tremor monitoring, Seismol. Res. Lett., 81(4), 664–669, doi:10.1785/gssrl.81.4.664.
Wech, A. G., and K. C. Creager (2008), Automatic detection and location of Cascadia tremor, Geophys. Res. Lett., 35, L20302, doi:10.1029/2008GL035458.
Wilson, D. S. (1993), Confidence intervals for motion and deformation of the Juan de Fuca Plate, J. Geophys. Res., 98, 16,053–16,071, doi:10.1029/93JB01227.
Xia, S., D. Zhao, and X. Qiu (2008), Tomographic evidence for the subducting oceanic crust and forearc mantle serpentinization under Kyushu, Japan, Tectonophysics, 449, 85–96, doi:10.1016/j.tecto.2007.12.007.
Yamamoto, Y., R. Hino, and M. Shinohara (2011), Mantle wedge structure in the Miyagi Prefecture forearc region, central northeastern Japan arc, and its relation to corner-flow pattern and interplate coupling, J. Geophys. Res., 116, B10310, doi:10.1029/2011JB008470.